ISTANBUL TECHNICAL UNIVERSITY ★ GRADUATE SCHOOL

URBANIZATION'S ROLE IN SHAPING TEMPERATURE RECORDS: INSIGHTS FROM IZMIR, TURKIYE

M.Sc. THESIS

Fatma Başak SAKA

Department of Meteorological Engineering

Atmospheric Sciences Programme

JULY 2024

ISTANBUL TECHNICAL UNIVERSITY ★ GRADUATE SCHOOL

URBANIZATION'S ROLE IN SHAPING TEMPERATURE RECORDS: INSIGHTS FROM IZMIR, TURKIYE

M.Sc. THESIS

Fatma Başak SAKA
(511211010)

Department of Meteorological Engineering

Atmospheric Sciences Programme

Thesis Advisor: Prof. Dr. Yurdanur ÜNAL

JULY 2024

İSTANBUL TEKNİK ÜNİVERSİTESİ ★ LİSANSÜSTÜ EĞİTİM ENSTİTÜSÜ

SICAKLIK REKORLARININ ŞEKİLLENMESİNDE KENTLEŞMENİN ROLÜ: TÜRKİYE, İZMİR'DEN ÇIKARIMLAR

YÜKSEK LİSANS TEZİ

Fatma Başak SAKA
(511211010)

Meteoroloji Mühendisliği Anabilim Dalı

Atmosfer Bilimleri Programı

Tez Danışmanı: Prof. Dr. Yurdanur ÜNAL

TEMMUZ 2024

Fatma Başak SAKA, a M.Sc. student of ITU Graduate School student ID 511211010 successfully defended the thesis/dissertation entitled “URBANIZATION'S ROLE IN SHAPING TEMPERATURE RECORDS: INSIGHTS FROM IZMIR, TURKIYE”, which she prepared after fulfilling the requirements specified in the associated legislations, before the jury whose signatures are below.

Thesis Advisor :	**Prof. Dr. Yurdanur ÜNAL** İstanbul Technical University	.....
Jury Members :	**Asst. Prof. Ceyhan KAHYA** Istanbul Technical University	.....
	Asst. Prof. Veli YAVUZ Samsun University	.....

Date of Submission : 24 May 2024
Date of Defense : 04 July 2024

The one she actually graduate,

FOREWORD

I want to start by thanking my thesis advisor, Prof. Dr. Yurdanur ÜNAL, for guiding me and being there for me throughout this long journey.

Next, I owe a huge thank you to my precious family and lovely friends, who have always been by my side, and to my colleagues from the EDF Trading Meteorology team, who have supported me throughout the intense workload to complete my master's thesis. Your support means a lot to me, and I feel incredibly lucky to have you in my life.

During the years I started and completed my master's degree, my life evolved rapidly in a completely different direction. I extend my greatest thanks to everyone who supported me throughout this entire process of adaptation and to myself for never giving up the fight, no matter how mentally and physically challenging it was.

June 2024

Fatma Başak SAKA
(Meteorological Engineer)

TABLE OF CONTENTS

Page

ABBREVIATIONS

CORINE **:** Coordination of Information on the Environment
NWP **:** Numerical Weather Prediction
UHI **:** Urban Heat Island
WRF **:** Weather Research & Forecasting

LIST OF TABLES

Page

LIST OF FIGURES

Page

URBANIZATION'S ROLE IN SHAPING TEMPERATURE RECORDS: INSIGHTS FROM IZMIR, TURKIYE

SUMMARY

The urban heat island concept was introduced to literature around the early 80s, when the construction of urban areas started to increase due to the increasing population of cities. The term urban heat island is defined as the temperature difference between urban and rural areas. From the early 80s until today, numerous studies have been conducted to deeply understand how the urban atmosphere interacts with its surroundings and how urban heat islands affect meteorological phenomena. Numerical weather prediction (NWP) models like The Weather Research and Forecasting (WRF) come in handy to simulate these phenomena. The WRF model is a sophisticated numerical weather prediction tool designed to serve atmospheric research and operational forecasting needs. As an NWP model, WRF utilizes mathematical equations representing atmospheric physics and dynamics to simulate weather patterns based on current observational data. Its versatility and modular structure allow for various applications, from short-term weather predictions to long-term climate studies. WRF stands out due to its high spatial and temporal resolution, which enables detailed simulations of meteorological phenomena at local, regional, and global scales. This model supports advanced data assimilation techniques and can integrate diverse data sources, enhancing its predictive accuracy. By providing detailed, reliable forecasts, WRF and other NWP models play a crucial role in weather-related decision-making, disaster preparedness, and environmental management, ultimately helping to safeguard lives and property. WRF model has significantly advanced the study of urban heat islands (UHIs) by providing high-resolution simulations of atmospheric conditions over urban areas. This numerical prediction model allows researchers to analyze the intricate interactions between urban landscapes and meteorological phenomenas such as heat waves and allows scientists to study the characteristics and impacts of UHIs more accurately.

In this study it was aimed to understand how urban heat island effect behavior of atmosphefric dynamics under heat wave conditions for 3rd most populas city of Turkiye, İzmir. Due to the mentioned advantages, it was decided to conduct the study using WRF model version 4.3. After preparing the necessary infrastructure and setting up the model, it was started to search the parameter set would work with. Based on the results of our previous studies within the same domain, parameterization set that best represents the region selected. One of the most critical aspects of the study was to run the model with land use information that accurately represents urbanization. Therefore, instead of using the default land use data, Coordination of Information on the Environment (CORINE) data used as the base for the model, thus laying the foundation for our study. We forced the model with ECMWF reanalysis data while running it and determined the case date using observational data provided by the Meteorological Directorate General. After selecting the date, we ran the model for July 2023, including the record-breaking day. Then, the outputs were compared with station

observations to see how closely the model's results matched actual data, and the effectiveness and accuracy of the model were assessed. After determining the model's performance, the performance of the parameterization set once again was validated. Then, the model ran again with the same settings, replacing the urban land use category in the CORINE data with the nearest rural area category. We analyzed the contributions of the interaction between the city and the atmosphere to the temperature on the record-breaking heat day by considering atmospheric boundary layer heights, temperature profiles, and atmospheric forces such as buoyancy. The study revealed that replacing urban areas with rural land use significantly altered the temperature of the area throughout the entire month. Notably, the minimum temperature difference between urban and rural areas during the record-breaking heat day occurred at night, consistent with the urban heat island effect. Additionally, there was a noticeable difference in boundary layer height when comparing urban and non-urban runs. During the record-breaking day, the buoyancy flux was higher for the urban run, while it was lower at night. This variation in buoyancy flux requires further investigation to fully understand the underlying mechanisms.

SICAKLIK REKORLARININ ŞEKİLLENMESİNDE KENTLEŞMENİN ROLÜ: TÜRKİYE, İZMİR'DEN ÇIKARIMLAR

ÖZET

Şehir Isı Adası kavramı, 80'lerin başlarında, şehir nüfusunun artmasıyla birlikte kentsel alanların inşasının artmaya başladığı dönemde literatüre girmiştir. Kentsel ısı adası terimi, kentsel ve kırsal alanlar arasındaki sıcaklık farkını tanımlamaktadır. 80'lerin başlarından günümüze kadar, kentsel atmosferin çevresiyle nasıl etkileşime girdiğini ve kentsel ısı adalarının meteorolojik olayları nasıl etkilediğini derinlemesine anlamak için sayısız çalışma yapılmıştır. The Weather Research and Forecasting (WRF) gibi sayısal hava tahmin (NWP) modelleri, bu olayları simüle etmek için oldukça kullanışlıdır. WRF modeli, atmosferik araştırma ve operasyonel tahmin ihtiyaçlarına hizmet etmek üzere tasarlanmış sofistike bir sayısal hava tahmin aracıdır.Bu model mevcut gözlemsel verilere dayanarak hava olaylarını simüle etmek için atmosfer fiziği ve dinamiklerini temsil eden matematiksel denklemleri kullanır. Çok yönlülüğü ve modüler yapısı, kısa vadeli hava tahminlerinden uzun vadeli iklim çalışmalarına kadar çeşitli uygulamalara imkan tanır. WRF, yüksek uzaysal ve zamansal çözünürlüğü sayesinde yerel, bölgesel ve küresel ölçeklerde meteorolojik olayların detaylı simülasyonlarını yapabilir. Bu model, gelişmiş veni asimilasyon tekniklerini destekler ve çeşitli veri kaynaklarını entegre edebilir, böylece tahmin doğruluğunu artırır. Detaylı ve güvenilir tahminler sağlayarak, WRF ve diğer NWP modelleri, hava ile ilgili karar alma, afet hazırlığı ve çevre yönetiminde kritik bir rol oynar, sonuçta hayatları ve mülkleri korumaya yardımcı olur. WRF modeli, kentsel ısı adalarının (UHI) çalışılmasında büyük ilerlemeler sağlamış olup, kentsel alanlar üzerindeki atmosferik koşulların yüksek çözünürlüklü simülasyonların hazırlanmasına ve incelenmesine kolaylık sağlamaktadır. Literatürde WRF modelinin kullanıldığı birçok farklı alanda çalışmalar yapılmış ve yapılmaktadır. Örneğin şehir ısı adası yoğunluğunun hesaplanmasında,,birçok farklı ölçekteki hava olayının modellenmesinde, sayısal hava tahmin modeli çıktılarının çözünürlüklerinin yükseltilmesinde bu model oldukça yaygın olarak kullanılmaktadır.

Bu çalışmada, Türkiye'nin en kalabalık 3. şehri olan İzmir'de, sıcak hava dalgası koşullarında şehir ısı adası etkisinin nasıl davrandığının anlaşılması amaçlanmıştır. Modelin sağladığı avantajlar ve literatüde bulunan başarılı çalışmalar göz önünde bulundurularak çalışmanın WRF modeli kullanılarak modellenmesine ve stabil güncel versiyon olan WRF version 4.3 kullanılmasına karar verilmiştir. Gerekli altyapı hazırlanıp model kurulumu tamamlandıktan sonra çalışılacak parametre seti araştırıldı, bu araştırma sırasında çalışma alanı için yapılan önceki çalışmalar, benzer coğrafi bölgeler ve iklim koşullarında yapılan yayınlar incelenerek. bölgeyi ve seçilen çalışma konusunu en iyi temsil eden model parametrizasyon seti seçildi.

CORINE, Avrupa Çevre Ajansı tarafından yürütülen ve arazi kullanım bilgilerini içeren bir projedir. CORINE arazi kullanım verisi, çeşitli çevresel uygulamalar için temel bilgi kaynağıdır ve 44 farklı arazi kullanım sınıfını içermektedir. Bu veri seti,

çevresel izleme, planlama ve yönetim süreçlerinde önemli bir rol oynar. Avantajları arasında, karar vericilere ve araştırmacılara geniş bir coğrafi alanda detaylı ve güncel bilgi sağlama kapasitesi bulunur. Ayrıca, Avrupa genelinde standardize edilmiş bir veri seti sunarak sınır ötesi çevresel yönetim ve politika geliştirme süreçlerini kolaylaştırır. CORINE verileri, çevresel değişikliklerin izlenmesi, arazi kullanım değişikliklerinin analiz edilmesi ve sürdürülebilir kalkınma politikalarının geliştirilmesine yönelik değerli bilgiler sunar. Çalışmanın en kritik yönlerinden biri, modelin, kentleşmeyi doğru şekilde temsil eden arazi kullanımı bilgileriyle çalıştırılmasıydı. Bu nedenle, varsayılan arazi kullanımı verileri yerine CORINE verilerinin modelin varsayılan koşulları kullanılarak değerlendirilmesi sağlandı. Sıcaklık rekoru kırılan Temmuz 2023 yılının istenilen koşullarak uygun olup olmadığının belirlenmesi için gözlem verileri analiz edildi. Sıcak hava dalgasının ve şehir ısı adasının etkilerinin incelenebilmesi için Meteoroloji Genel Müdürlüğü tarafından sağlanan gözlem verileri bölgesel ortalama ve noktasal istasyon değerleri incelenirken sinoptik patternde tespiti için Avrupa Orta Vadeli Hava Tahminleri Merkezi (ECMWF) ERA5 verilerinden faydalanıldı.

ERA5,ECMWF tarafından geliştirilen ve küresel atmosferik verilerin yeniden analizini içeren bir veri setidir. ERA5 reanaliz verisi, 1979'dan günümüze kadar olan dönemi kapsar ve atmosferik, yüzeysel ve deniz parametrelerine dair yüksek çözünürlüklü bilgiler sunar. Bu veri setinin avantajları arasında, iklim araştırmaları ve hava durumu analizleri için güvenilir ve detaylı bir temel sağlaması bulunur. ERA5, yüksek zaman çözünürlüğü (saatlik veriler) ve yüksek mekansal çözünürlüğü (31 km grid aralığı) ile kullanıcılara çok hassas ve kapsamlı bilgi sağlar. Ayrıca, uzun bir zaman dilimini kapsaması, iklim değişikliği trendlerinin ve ekstrem hava olaylarının analizine olanak tanır. ERA5 verileri, hava tahminleri, tarım, su kaynakları yönetimi, enerji sektörü ve afet yönetimi gibi birçok alanda uygulama bulur ve bilimsel araştırmalara önemli katkılar sunar.

Seçilen Temmuz 2023 ayı içerisinde şehir ısı adasının en yoğun olduğu dönemlerin sıcaklık rekoru ile örtüştüğü ve sinoptik paternin bu koşulları desteklediği göz önüne alınarak 2023 Temmuz ayının simülasyonlar için uygun koşulları barındırdığına karar verildi. Model başlangıç koşulları için yapılmış önceki çalışmalarda gösterdiği başarıdan yola çıkarak ECMWF ERA5 tek seviye ve basınç seviyeleri verileri temin edilerek modele girdi olarak verildi ve belirlenen model parametre seti ile birlikte rekor kıran günü de içeren Temmuz 2023 ayı için model çalıştırıldı. Elde edilen çıktılar gözlem değerleriyle karşılaştırılarak seçilmiş performans metrikleri ve Taylor diyagramları hazırlanarak modelin performansı değerlendirildi ve parametre setinin performansı tekrar doğrulandı. Ardından, aynı veri ve parameter seti ile hazırlanan model başlangıç koşulları CORINE verilerindeki kentsel arazi kullanım kategorisi en yakın kırsal alan kategorisiyle değiştirilerek tekrar çalıştırıldı. Modelin Temmuz 2023 ve rekor kıran sıcaklık gününde, şehir ve atmosfer arasındaki etkileşimin sıcaklığa katkıları atmosferik sınır tabakası yükseklikleri, sıcaklık profilleri analiz edildi.

Çalışmanın sonuçları incelendiğinde, kentsel alanların kırsal arazi kullanımı ile değiştirilmesinin, tüm ay boyunca bölgenin sıcaklığını önemli ölçüde değiştirdiğini ortaya koydu. Özellikle, rekor kıran sıcaklık gününde kentsel ve kırsal alanlar arasındaki minimum sıcaklık farkının gece meydana geldiği, bu durumun kentsel ısı adası etkisiyle tutarlı olduğu anlaşıldı. Ayrıca, kentsel ve kentsel olmayan koşullar arasında sınır tabakası yüksekliğinde belirgin bir fark olduğu görüldü.

Literatürden yola çıkarak seçilen atmosferdeki yukarı yönlü hareket akısı bu çalışma için yatay kesti alanı üzerinden hesaplanarak şehir varken ve yokken akıda oluşan fark

incelendi. Rekor kıran gün boyunca, yukarı yonlü hareket akısının kentsel koşul için daha yüksekken, gece daha düşük olduğu belirlendi. Bu kaldırma akısı varyasyonunun, altta yatan mekanizmaları tam olarak anlamak için daha fazla araştırma gerektirdiği sonucuna varıldı.

1. INTRODUCTION

In the context of a changing and evolving world, population growth has significantly altered the interaction between humans and the atmosphere. This shift has prompted scientists to investigate human-atmosphere interactions more thoroughly, including anthropogenic changes in atmospheric conditions, one example of this phenomenon is the concept of the urban heat island which can be defined as the temperature difference between urban and rural area. Howard et al. (1983) were the first to observe that cities are warmer than rural areas. This phenomenon arises due to human interactions such as dense urbanization, asphalt roads, concrete buildings, and industrial activities, which alter the absorption and reflection properties of solar radiation, significantly impacting the environmental temperature profile (Oke, 1982).

The effects of the urban heat island are particularly pronounced on the temperature profile within urban areas. Urban heat island intensity can be calculated with equation:

$$T_{Urban} - T_{Rural} \tag{1.1}$$

Oke (1987) demonstrated that temperature differences between urban and rural areas, especially during nighttime, increase significantly.This increase is a consequence of urban development and thermal properties of the materials used in the urban environent.. Additionally, the impacts of this phenomenon on microclimates should not be overlooked. Microclimate refers to the small-scale weather conditions of a particular area, and the urban heat island can substantially influence these conditions (Grimmond & Oke, 1999). There are various methods available for researching these conditions, such as examining observational data, conducting simulations to analyze the effects of changing conditions, and other analytical techniques. These studies and researches mainly focus on the layer of the atmosphere called the boundary layer. Urban atmosphere and the boundary layer within it are critical to understanding how cities influence local weather and climate. The urban boundary layer is the lowest part of the atmosphere that directly interacts with the urban surface and is characterized by turbulent mixing and distinctive temperature profiles due to the urban heat island effect (Oke, 1987). This layer is influenced by factors such as building density and heights,

surface materials, and human activities, all of which lead to higher temperatures, altered wind patterns, and increased pollution levels compared to rural areas (Roth, 2000). The complexity of the urban boundary layer makes it essential that urban climate models represent these interactions to effectively predict weather patterns and air quality in cities. This environment often experiences the urban heat island effect, causing higher temperatures compared to surrounding rural areas (Oke, 1982).

1.1 Atmospheric Boundary Layer and Heatwaves

The atmospheric boundary layer is the lowest part of the atmosphere, directly influenced by the Earth's surface in contact with, where friction, heat and moisture exchanges occur. It typically extends from the ground up to about 1-2 kilometers but can vary significantly depending on weather conditions and terrain (Stull, 1988).

The surface layer, which can be seen as a dashed red line in Figure 1.1, is the bottom of the boundary layer, typically extending up to 10 m above the ground, which is characterized by strong vertical changes of atmospheric variables such as humidity temperature and wind speed. Turbulence in this layer is primarily driven by surface friction and heat fluxes (Garratt, 1992). Above the surface layer lies the mixed layer, which can extend several hundred meters to a few kilometers above the ground. In this layer, turbulence is more uniform, resulting in well-mixed conditions where temperature and moisture are relatively constant with height. During the daytime, the mixed layer grows due to convective processes driven by solar heating of the ground (Stull, 1988). As the sun heats the surface of the Earth, the temperature of the air near the ground increases, causing it to rise and create convection currents. This convective activity enhances the mixing of air within the boundary layer, leading to an increase in the height of the mixed layer as the day progresses. At the top of the mixed layer is the entrainment zone, a crucial region where the turbulent boundary layer interacts with the free atmosphere above. This zone is characterized by a decrease in turbulence compared to the more turbulent mixed layer below . Additionally, there is a sharp gradient in temperature and humidity which distinguishes the entrainment zone from the layers above and below it. This temperature and humidity gradient is indicative of the mixing processes occurring in this region.

The entrainment zone acts as a boundary where air from the free atmosphere is incorporated into the boundary layer below. (Stull, 1988). This mixing process is

essential for the transfer of properties such as heat, moisture, and momentum between the free atmosphere and the boundary layer. As a result, the entrainment zone plays a critical role in regulating the overall structure and dynamics of the boundary layer, influencing weather patterns and climate processes.

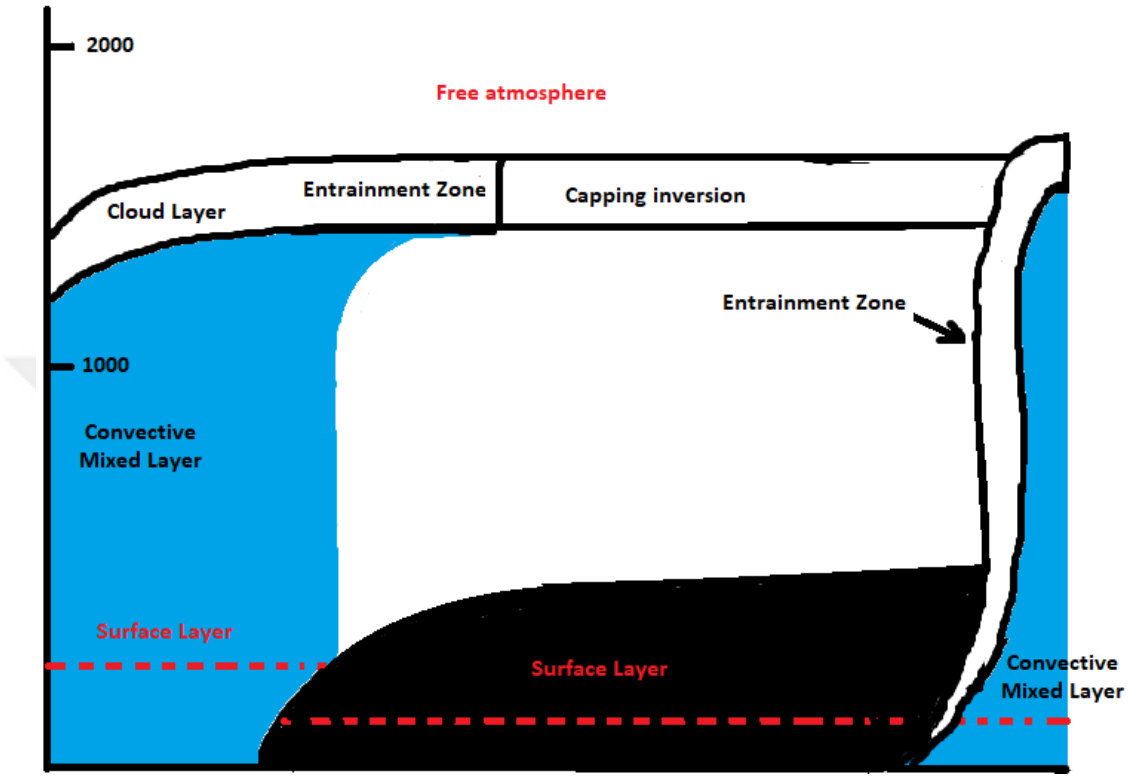

Figure 1.1 : Schematic representation of atmospheric boundary layer.

The free atmosphere is the region above the boundary layer, starting from the top of the boundary layer (typically marked by the entrainment zone) and extending upwards. Unlike the boundary layer, the free atmosphere is relatively unaffected by the direct influence of the Earth's surface, such as friction and surface heating. Turbulence in the free atmosphere is generally less intense and more intermittent than in the boundary layer, and atmospheric motions are dominated by large-scale synoptic and mesoscale processes rather than surface-induced turbulence (Stull, 1988). This region is crucial for large-scale weather patterns and is where most weather phenomena like heatwaves related.

A heatwave is typically defined as a prolonged period of excessively hot weather, often accompanied by high humidity levels. According to the National Oceanic and Atmospheric Administration (NOAA), a heatwave is characterized by temperatures that are significantly above the average for a specific region during that time of year,

lasting for an extended period, usually several days or more. The World Meteorological Organization (WMO) defines a heatwave as "a period of marked unusual hot weather," noting that the threshold for what constitutes "unusual" varies depending on the local climate and average temperatures (World Meteorological Organization, 2023). Heatwaves can vary in intensity and duration but are characterized by their ability to cause discomfort, heat-related illnesses, and even mortality, especially in vulnerable individuals such as the elderly and young children. Heatwaves interact with the atmosphere in various ways, impacting weather patterns and atmospheric dynamics. They can intensify due to atmospheric blocking patterns, where a stable high-pressure system traps hot air for an extended period, preventing the dispersion of heat (Trenberth & Shea, 2006). Additionally, the urban heat island effect, caused by human activities and infrastructure in urban areas, can further elevate temperatures locally and influence atmospheric circulation (Oke, 1982). Understanding the mechanisms and impacts of heatwaves is crucial for climate adaptation and resilience planning, as their frequency and severity are expected to increase with ongoing climate change (IPCC, 2021).Türkiye, located at the crossroads of Europe and Asia, experiences periodic heatwaves that significantly impact its climate and environment. Heatwaves in Türkiye are characterized by prolonged periods of excessively high temperatures, often exceeding normal seasonal averages, which can lead to serious health risks, particularly for vulnerable populations such as the elderly and those with pre-existing health conditions. These extreme heat events are exacerbated by factors such as urbanization, which contributes to the urban heat island effect in cities like Istanbul and Ankara, where temperatures can be several degrees higher than surrounding rural areas (Özdemir et al., 2020). Climate change is also playing a role in increasing the frequency and intensity of heatwaves across the region (Yücel et al., 2017).

1.2 Buoyancy Flux Index

The buoyancy flux index is a quantitative measure used to evaluate the strength and effects of buoyancy-driven processes in the atmospheric boundary layer. This index is derived from the buoyancy flux, which represents the vertical transfer rate of buoyancy—essentially the product of vertical velocity and temperature fluctuations within a given atmospheric layer (Stull, 1988). The buoyancy flux index helps assess

the convective activity and turbulence within the boundary layer, providing insights into the stability and vertical mixing of the atmosphere.

A high buoyancy flux index indicates strong surface heating, leading to significant upward transport of warm air and enhanced convective mixing. This is often observed during the daytime when solar radiation heats the ground, causing the air above to become buoyant and rise (Garratt, 1992). Conversely, a low or negative buoyancy flux index suggests weaker convective activity or even stable conditions, often occurring at night or during surface cooling periods, suppressing vertical motion and reducing turbulence.

Urbanization influences the land surface properties by affecting absorption and reflection of short wave radiation, emission of longwave radiation, and infiltration and storage of energy. These changes in urban environments create a bouyancy-driven atmospheric circulation. The buoyancy flux index is crucial in various meteorological and environmental applications as it aids in predicting the development of clouds and precipitation, understanding the dispersion of pollutants, and modeling the urban heat island effect. In urban areas, where surface characteristics significantly differ from rural regions, the buoyancy flux index helps understand how built environments influence local weather patterns and air quality (Roth, 2000). By providing a clear metric for evaluating vertical mixing and thermal dynamics, the buoyancy flux index is an essential tool in atmospheric science and urban climate studies.

The buoyancy flux equation (Garrat,1994) is given below:

$$B_0 = \overline{w'b'}_{z=0+} = \frac{g}{\rho c_p \bar{T}}\left(SF + 0.61\frac{c_p \bar{T}}{L}\, LF\right) \tag{1.2}$$

In this equation, T represents air temperature, SF represents sensible heat flux, LF represents latent heat flux, g represents the gravitational constant, ρ represents air density, and Cp represents the specific heat at constant pressure. Positive buoyancy flux is related to upward motion, convection, and atmospheric mixing (daytime heating), while negative buoyancy flux is related to downward motion, stable conditions, and limited mixing (nighttime cooling or stable conditions).

This study aims to assess the effects of the urban heat island intensity on the boundary layer and temperature structure over İzmir, Türkiye, specifically on days with record-breaking temperatures.

1.3 Literature Review

The changes of the atmospheric boundary layer during heat wave conditions have been the subject of numerous studies, each employing various approaches. In July 2016, during the heat wave episode in New York, examination of the boundary layer temperature profiles shows elevated temperatures which were observed throughout much of the boundary layer between 800 and 2500 meters. The urban heat island intensity of the megacity reached approximately 10 degrees, almost double the 10-year average. (Ramamurthy, González, Ortiz, Arend, & Moshary, 2017). Chen, Boomsma, and Holmes (2023) conduct a multiscale analysis of heatwaves and urban heat islands (UHIs) in the western United States during the summer of 2021. The study examines the spatial and temporal patterns of heatwaves and their interaction with UHIs. Findings indicate that heatwaves intensify UHIs, exacerbating temperature extremes in urban areas compared to rural surroundings. The research underscores the importance of addressing urban planning and climate adaptation strategies to mitigate the compounded effects of heatwaves and UHIs. The study by Ramamurthy and Bou-Zeid (2016) explores the interaction between heatwaves and urban heat islands (UHIs) across multiple cities. Using advanced modeling techniques, the research investigates how UHIs vary in intensity among cities with different geo-physical characteristics. Findings show that the amplitude of UHIs is related to the physical size of the city. However, cities of similar sizes can respond differently to heatwaves. Specifically, in New York City, Washington, DC, and Baltimore, UHIs are more pronounced during heatwaves compared to smaller cities, a pattern not observed in Philadelphia. The study underscores that UHI patterns and their interaction with heatwaves are influenced by dynamic factors.

Furthermore, recent studies employing the Weather Research and Forecasting (WRF) model have provided valuable insights into the dynamics of the urban heat island. This study by Bilang et al. (2024) evaluates the performance of the Weather Research and Forecasting (WRF) Model, coupled with various urban canopy models (UCMs), in simulating 2 m air temperature and 2 m relative humidity in Metro Manila during a high heat event in April 2018. The study compares simulation results with observations from weather stations and identifies the presence of urban heat islands, particularly in the northwest and central areas during the day and across Metro Manila at night. The results show that the WRF model accurately simulates air temperature with an RMSE

of less than 3.0°C, a mean bias error of less than 2.0°C, and an index of agreement of over 0.80. However, it faces challenges in accurately simulating relative humidity. The addition of UCMs does not necessarily improve temperature simulations, while the BEP model improves relative humidity simulation. The study also highlights the significance of using actual urban morphology values in the WRF model for accurate near-surface variable simulations. Another study conducted by Smith et al. (2015) utilized the WRF model to simulate the urban heat island effect in Los Angeles, revealing the interactions between urban morphology and temperature profiles. Similarly, Chen et al. (2018) use the WRF to examine the effects of land use changes on Beijing's urban heat island intensity, highlighting the importance of land cover characteristics in modulating temperature differences. Another study conducted by Rajeswari et al. (2021) aimed to analyze how boundary layer parameters change for Chennai, a coastal city over the tropics. The study is calculated the differences in buoyancy fluxes to capture turbulence characteristics between urban and non-urban scenarios. Kong et al. (2023) investigate the impact of heatwaves (HWs) on urban heat islands (UHIs) in Greater Sydney, focusing on changes in the surface energy budget across different land types during a 2020 HW event. Using the Advanced Weather Research and Forecasting (WRF) model, the study finds that HWs intensify nighttime surface UHI by about 4°C. They find that urban areas store more heat due to higher solar radiation absorption and reduced evapotranspiration, with maximum heat storage fluxes around 200 W/m² higher during HW than post-HW. In contrast, forests and savannas show lower heat storage fluxes. The study also notes that other meteorological conditions, such as strong hot and dry winds, influence the air temperature pattern, leading to higher temperatures in both urban and forested areas. These findings can aid in developing strategies for mitigating UHI effects during heatwaves.

Another study conducted for North America, two different WRF (Weather Research and Forecasting) simulations were designed: one with urban parametrization (Urban Canopy model) and the other without it. The findings indicated that urban heat islands intensify heatwaves by increasing the height of the turbulent boundary layer, altering urban surface energy budget, and affecting regional winds. The shift in energy from latent to sensible heat fluxes, along with the resulting changes in the urban planetary boundary layer, tends to enhance the intensity, extent, and duration of widespread

heatwaves (Garuma, G. F. , 2022). Modelling skills of WRF model is also very important for capturing realistic conditions to analyse. Roukounakis et al. (2023) conducted high-resolution WRF modeling to analyze extreme heat events and map the Urban Heat Island (UHI) characteristics in Athens, Greece. The study found a strong correlation between WRF output and observed temperatures, with R values ranging from 0.80 to 0.93 and an average mean absolute bias of 1.5 °C. Same research also revealed the intensity and spatiotemporal variability of the UHI effect, with magnitudes sometimes reaching 8–9 °C. Chew, Liu, Li, and Norford (2023) examine the interaction between heatwaves and urban heat island (UHI) effects in Singapore during an April 2016 heatwave using ground observations and the Weather Research and Forecasting (WRF) model. Their findings show that while daytime temperatures can be 3°C higher during heatwaves, the UHI intensity remains stable at approximately 2.5°C, with no significant amplification during heatwaves. The WRF model simulations support these observations, indicating no heatwave-UHI synergy. The study also finds no notable changes in wind speed, soil moisture, or heat storage flux during the heatwave, suggesting that the heatwave-UHI interaction in tropical cities may differ from that in temperate regions.

Among the studies in the literature, there are also results showing that the urban heat island does not change during the heat wave event such as ,a study conducted by Shu et al.(2023) using WRF model to determine how the urban heat island was affected during the heat wave event for Montreal and Ottawa. According to the results obtained, it was observed that the city's surface temperature increased by up to 12 ℃ and the air temperature near the surface by up to 6 ℃, and the intensity of the urban heat island did not increase during the heat wave and even decreased slightly in the daily cycle. On the other hand some studies investigating the effects of urbanization and heat waves have not yielded certain results. For instance, Silva et al.,(2022) considering RCP 8.5 scenarios, simulated a future scenario for Lisbon using a method similar to our targeted study. Using the Weather Research and Forecasting model (WRF) coupled with the Single-layer Urban Canopy Model (SLUCM), results show that urban irrigation effects offset anthropogenic heat by increasing latent heat release. While the results prove that the urban heat island effect intensifies at night, no definitive conclusions have been reached regarding the impact of heatwaves. The fact that this study does not give a definitive result like others may be related it’s methodology is

different and it takes future scenarios into consideration thus researches that continued the study method as a case study were able to capture the effects of heat waves and urbanization.

In recent years, Türkiye has witnessed a notable increase in the intensity of heatwaves, a trend attributed largely to climate change. In their study Unal et al, 2013, examines the impact of global warming on heat waves in western Turkey from 1965 to 2006. It identifies an increase in the frequency and duration of heat waves, especially after 1998. The research also explores correlations between hot days and sea surface temperatures in the Mediterranean and Black Seas, as well as the relationship between heat waves and fire occurrences. Heatwaves in Türkiye are becoming more frequent, lasting longer, and reaching higher temperatures than in previous decades. This trend has significant implications for public health, agriculture, and energy demand across the country. Urban areas like Istanbul and Izmir are particularly vulnerable due to the urban heat island effect, where densely built environments retain more heat, exacerbating already elevated temperatures during heatwave events (Çınar et al., 2021, Unal et al., 2020, Saka & Unal, 2024). Analyzing and taking necessary measures against these increasingly frequent and impactful natural events is highly important which is the main motivation for this study.

2. METHODS

In this section, the methodology decided for the study after the literature review and research will be explained and the data and methods used throughout the study will be described.

2.1 Area of Study

Izmir, located on the western coast of Türkiye along the Aegean Sea, features diverse topography and rich geographical characteristic which can be seen seen from Figure 2.1. The city is surrounded by mountain ranges, including the Yamanlar and Spil Mountains, contributing to its varied landscape. The Gediz River, which flows into the Gulf of Izmir, is significant for the region's hydrology. The coastline is dotted with bays and peninsulas, creating a scenic and irregular shoreline.

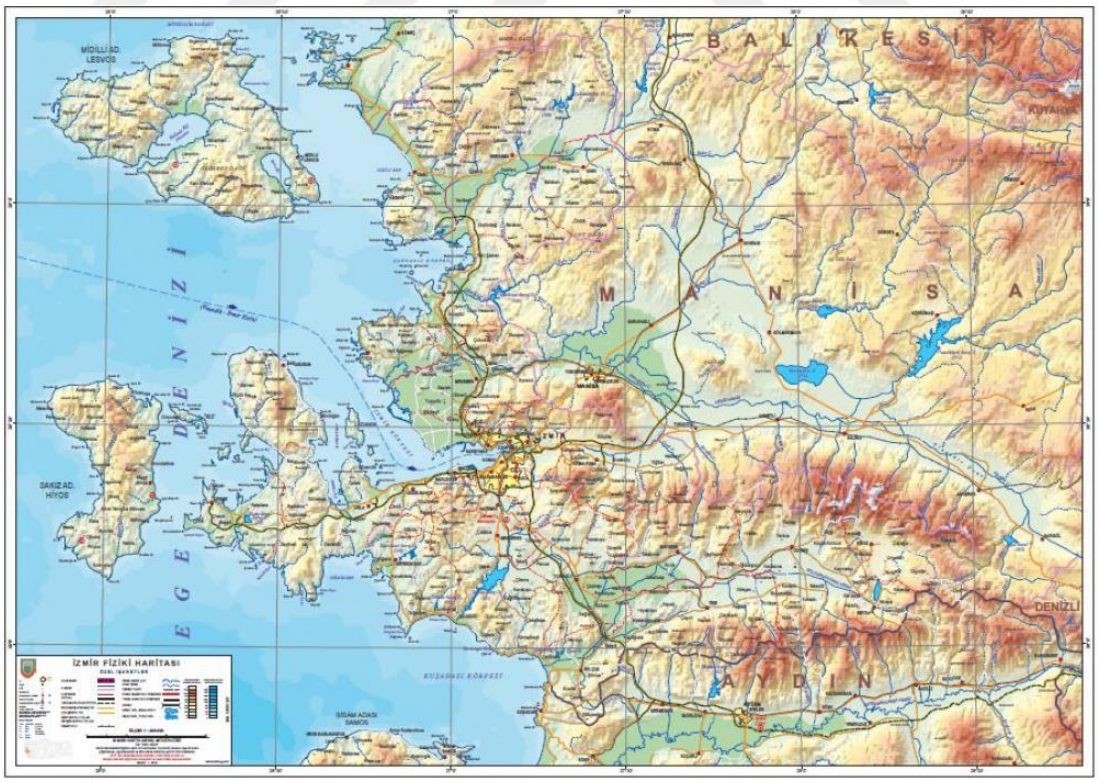

Figure 2.1 : Physical Topography Map of Izmir (retrieved from :Republic of Türkiye Ministry of National Defence Directorate General for Mapping).

The population density of İzmir has shown significant changes over the years. Since 2000, the city has experienced rapid growth, becoming a major metropolitan area. As of 2020, İzmir's population reached approximately 4.3 million, reflecting the city's economic and social appeal. Located on the western coast of Türkiye along the Aegean Sea, İzmir's strategic location has played a key role in its population density increase. There are variations in population density across different districts of the city, with central areas such as Konak, Karşıyaka, and Bornova having higher densities.This growth has necessitated the expansion of infrastructure, housing, and services in the city and increasing urbanization yet population density over time reached up to 400 (person over km^2 area) which can be seen from Figure 2.2

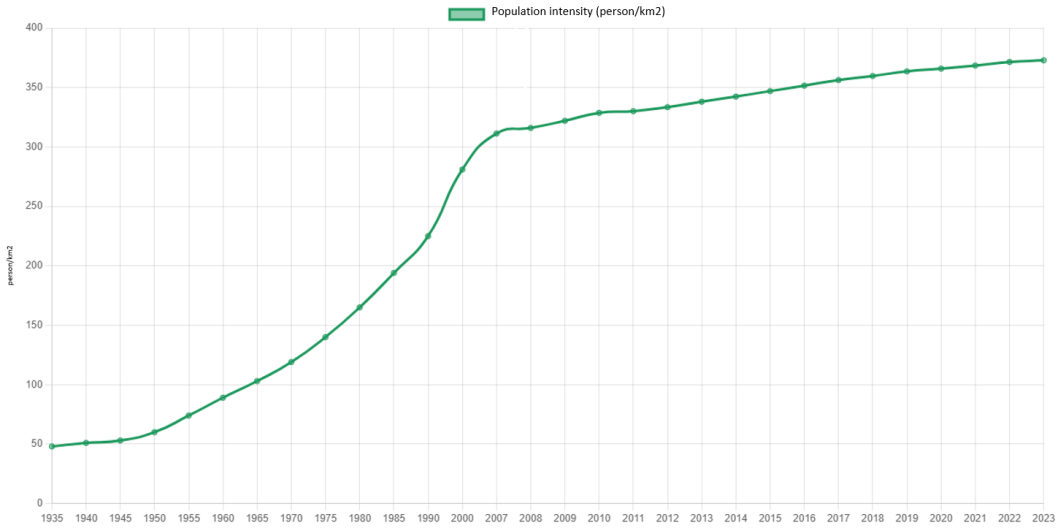

Figure 2.2 : Population intensity over km2 area for Izmir,Türkiye retrieved from (Url-1).

In July 2023, Izmir recorded unprecedented high temperatures, breaking its previous records. The city experienced extreme heat on 26^{th} of July 2023 for the period of 1983-2023 as 43.2°C which is also highest record for the year. This intense heat wave significantly impacted daily life, leading to increased health risks and putting a strain on energy resources due to the high demand for cooling. Overall we believe considering the population density and urbanization rate, Izmir provides suitable conditions for our study and needs further investigations.

2.2 Data

Multiple data sources are used during this study for different purposes. Case period selection conducted using the data at 68 observation stations which are provided from

Turkish State Meteorological Service. The distribution of the stations are given in the Figure 2.3 and the list of stations are given in Table 2.1. The same data also used while evaluating model performance and further analysis.

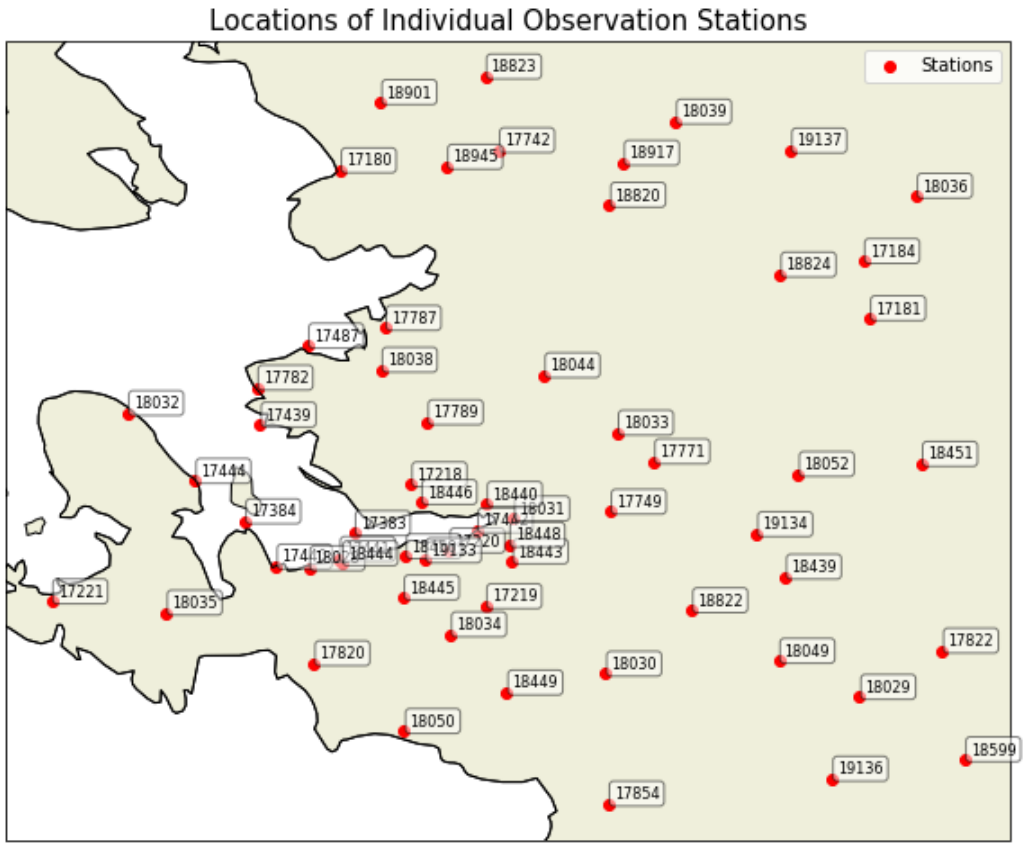

Figure 2.3 : Map of observation stations.

Table 2.1 : Table of observation station from state meteorology.

Istasyon_No	Istasyon_Adi	enlem	boylam
17181	AKHİSAR HAVALİMANI	38.8095	27.834
17184	AKHiSAR	38.9118	27.8233
17771	ŞEHZADELER/SPİL DAGI MİLLİ PARKI	38.5538	27.4484
18033	MANiSA KENT ORMANI	38.6051	27.3833
18036	AKHiSAR/KARAKÖY ORMAN DEPOSU	39.0283	27.9175
18039	SOMA/CENKYERi ORMAN SAHASI	39.1608	27.4871
18044	YUNUSEMRE/ÇAKMAK ORMAN SAHASI	38.7077	27.2522
18824	AKHİSAR/MECİDİYE BELDESİ	38.8875	27.6739
17180	DİKİLİ	39.0737	26.888
17218	ÇİĞLİ HAVALİMANI	38.5127	27.0144
17219	İZMİR ADNAN MENDERES HAVALİMANI	38.295	27.1481
17220	İZMİR BÖLGE	38.3945	27.0821
17221	ÇEŞME	38.3036	26.3724
17383	NARLIDERE/İZMİR KÖRFEZİ A NOKTASI IŞIKLI ŞAMANDIRA	38.4256	26.9133
17384	URLA/KUBİLAY SIĞLIĞI IŞIKLI ŞAMANDIRA	38.4467	26.7175
17439	AZAPLAR (VENEDİK) KAYALIĞI FENERİ	38.6194	26.7447
17440	URLA BALIKÇI BARINAĞI MENDİREK FENERİ	38.3658	26.7733
17441	GÜZELBAHÇE FENERİ	38.3794	26.8861

Table 2.1 (continued) : Table of observation station from state meteorology.

Istasyon_No	Istasyon_Adi	enlem	boylam
17442	KONAK/İZMİR PASAPORT MENDİREK FENERİ	38.4303	27.1322
17444	KARABURUN/MORDOĞAN ANA MENDİREK (KUZEY) FENERİ	38.5189	26.6283
17487	FOÇA TRAFİK GÖZETLEME KEGM	38.7605	26.8299
17742	BERGAMA	39.1098	27.171
17749	KEMALPAŞA	38.4639	27.3705
17782	FOÇA TOPRAK SU	38.6856	26.7392
17787	ALİAĞA	38.7922	26.9682
17789	MENEMEN	38.6237	27.0433
17820	SEFERİHİSAR	38.19306	26.84097
17822	ÖDEMİŞ	38.2157	27.9642
17854	SELÇUK	37.9423	27.3669
18028	URLA	38.3628	26.8322
18029	TİRE	38.133	27.8165
18030	TORBALI	38.1743	27.3623
18031	BORNOVA/ZEYTİNCİLİK ARŞ.(TAGEM)	38.4517	27.1979
18032	KARABURUN	38.6401	26.5081
18034	MENDERES ORMAN SAHASI	38.2447	27.0849
18035	URLA/UZUNKUYU ORMAN SAHASI	38.2836	26.577
18038	ALİAĞA/BOZKÖY ORMAN SAHASI	38.7175	26.9613
18049	BAYINDIR	38.1975	27.6719
18050	MENDERES/GÜMÜLDÜR	38.072	27.0026
18052	TURGUTLU	38.5312	27.7065
18439	KEMALPAŞA/OVACIK KÖYÜ	38.3478	27.6836
18440	BAYRAKLI	38.4778	27.1489
18443	BUCA	38.375	27.1953
18444	GÜZELBAHÇE	38.3717	26.8908
18445	İZMİR ÇATALKAYA RADAR SAHASI	38.3106	27.0006
18446	KARŞIYAKA	38.4811	27.0322
18448	KONAK	38.4049	27.1895
18449	MENDERES/ÇİLEME KÖYÜ	38.1408	27.1858
18450	NARLIDERE	38.3842	27.0044
18451	AHMETLİ	38.5492	27.9269
18599	ÖDEMİŞ/DEMİRDERE KÖYÜ	38.0214	28.0042
18820	KINIK/KÖSELER KÖYÜ	39.0122	27.3694
18822	BAYINDIR / ÇINARDİBİ KÖYÜ	38.2878	27.5161
18823	BERGAMA/İNCECİKLER ORMAN SAHASI	39.2414	27.1475
18901	DİKİLİ/ÇUKURALAN KÖYÜ	39.1956	26.9606
18917	KINIK	39.08723	27.393908
18945	BERGAMA/ÇAMKÖY	39.08006	27.0782
19133	BALÇOVA	38.37694	27.04008
19134	KEMALPAŞA/BAĞYURDU KÖYÜ	38.42365	27.63237
19136	TİRE/SOMAK KÖYÜ	37.98674	27.76669
19137	KIRKAĞAÇ	39.10911	27.69309

Model forced with ERA5 reanalysis pressure and single level hourly data provided by ECMWF (Hersbach et al.,2023). The ERA5 dataset, produced by the European Centre for Medium-Range Weather Forecasts (ECMWF) for the Copernicus Climate Change Service, offers a detailed reanalysis of global atmospheric, land surface, and ocean wave conditions from 1950 to near real-time. It combines historical observational data

with modern weather forecasting models to provide a consistent and complete climate record. ERA5 includes data at single and multiple levels. Single level data covers surface parameters like temperature and precipitation, while multiple level data includes atmospheric variables at different heights, such as wind and humidity. This dataset is crucial for climate monitoring, weather forecasting, and studying historical weather events. ERA5 data is available hourly and can be accessed through the Copernicus Climate Data Store (CDS) for fast retrieval or ECMWF's MARS archivefor complete datasets. Its comprehensive coverage makes ERA5 essential for analyzing climate trends and weather patterns over the past decades (ECMWF Confluence page).

The CORINE (Coordination of Information on the Environment) land use dataset, created by the European Environment Agency (EEA), provides detailed and consistent information on land cover across Europe. It was initiated in 1985 by the European Commission with the aim of gathering consistent and comparable information on land cover and land use across Europe. The classification system used is hierarchical and consists of multiple levels, with the most detailed level providing up to 44 different land cover classes, offering high-resolution insights into the spatial distribution of urban zones, agricultural fields, forests, and bodies of water (Büttner et al., 2004). The CORINE land cover data has been produced for several reference years: 1990, 2000, 2006, 2012, and 2018. This allows for the analysis of land cover changes over time. The data is provided at a scale of 1:100,000, with 100 meters resolution. The data set is publicly accessible and can be downloaded from the European Environment Agency's website. Due to its precision and consistency across various regions, CORINE data is extensively utilized in environmental research, urban planning, and land management. It is beneficial for urban heat island (UHI) modeling, as it enables researchers to accurately depict the complexity of urban environments, thereby enhancing the reliability of atmospheric and climate simulations (Bossard et al., 2000).

2.3 Case Selection

As mentioned at the previous sections in July 2023, Izmir experienced extreme heat on 26th of July 2023 for the period of 1983-2023 as 43.2°C which is also highest record for the year. Before determining a date range for the study, we took a step back and examined the difference in July 2023 temperature values and synoptic pattern

compared to previous years. Ventura et al. (2023) conducted a study analyzing synoptic weather patterns of heatwave events, focusing on the Iberian Peninsula and the Metropolitan Area of Barcelona as case studies. They utilized multivariate analysis to identify patterns using mean sea level pressure, geopotential height at 500 hPa, and maximum daily 2 m temperature data from HW events between 1950 and 2020.

In order to get an idea about the synoptic pattern, we wanted to determine the monthly average dominant pattern of the 500 hpa Geopotential data. Since we chose to perform synoptic pattern analysis rather than classification in our study, we examined 500hpa geopotential height values with reference to this study at Figure 2.4. Geopotential height, a measure of the altitude at which a given pressure level occurs in the atmosphere, plays a crucial role in the dynamics of heatwaves. Higher geopotential heights are often associated with the presence of high-pressure systems, which can lead to prolonged periods of clear skies, reduced cloud cover, and increased solar radiation reaching the Earth's surface (Stefanon, M. Et al. ,2012). When Figure 2.4 is examined considering this information, it is seen that 2023 has the highest values of the high pressure area that affects the southwest of Türkiye compared to the last 10 years. Considering that high pressure values on the monthly average geopotential height values map tend to increase the effect of the heat wave, it seems that the dominant synoptic pattern of July 2023 supports dry and warm potentially record breaking conditions through the month.

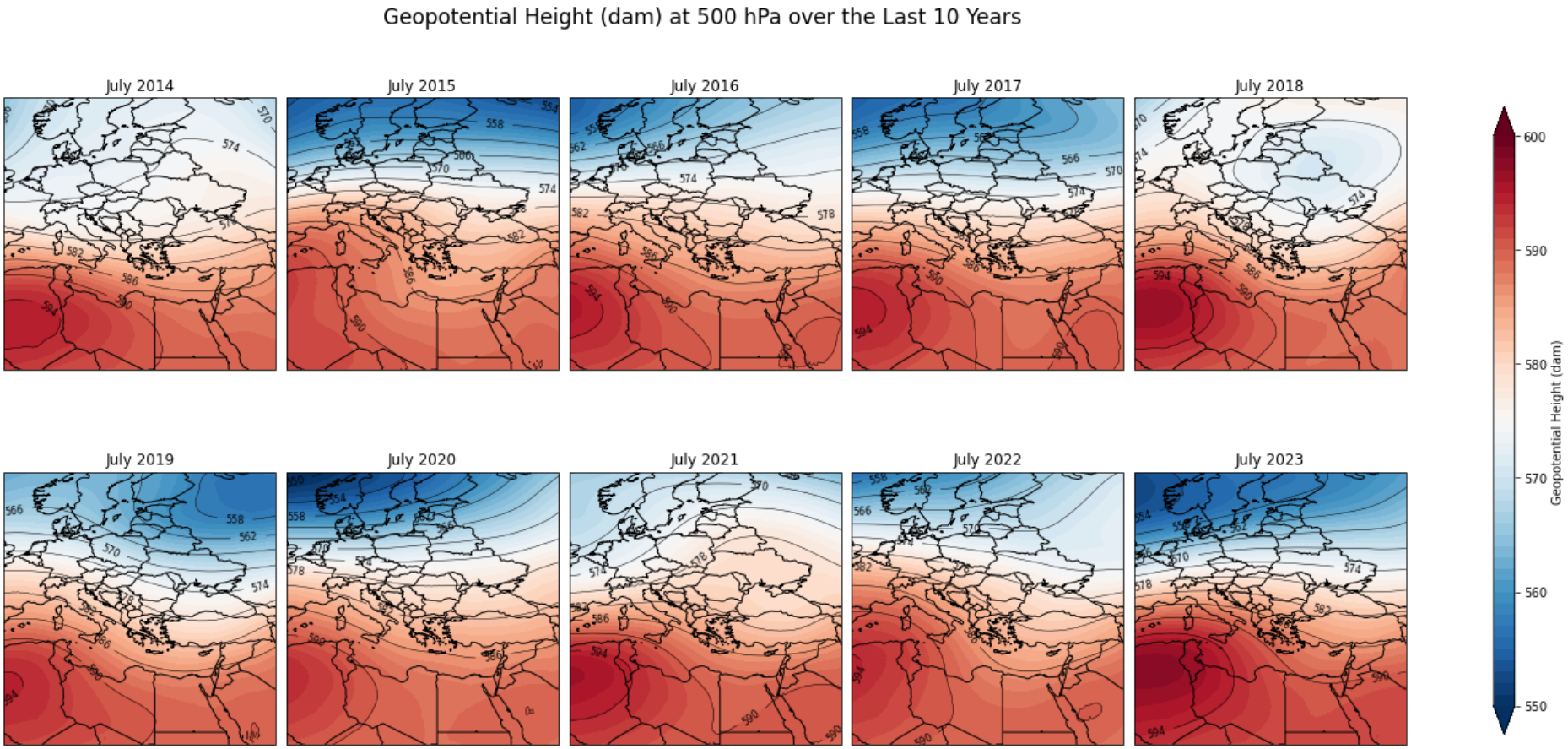

Figure 2.4 : Monthly average 500 hpa geopotential height values from ERA5 pressure level dataset.

After determining that the synoptic pattern supported the observed conditions, we examined the daily average temperature and relative humidity parameters from the station data obtained from the State Meteorology. In Figure 2.5, it is observed that the temperature values throughout the month ranged between 24 and 31 degrees Celsius, while the relative humidity values were above 40% between the 1st and the 9th days of the month, but did not fall below 40% for the rest of the month.

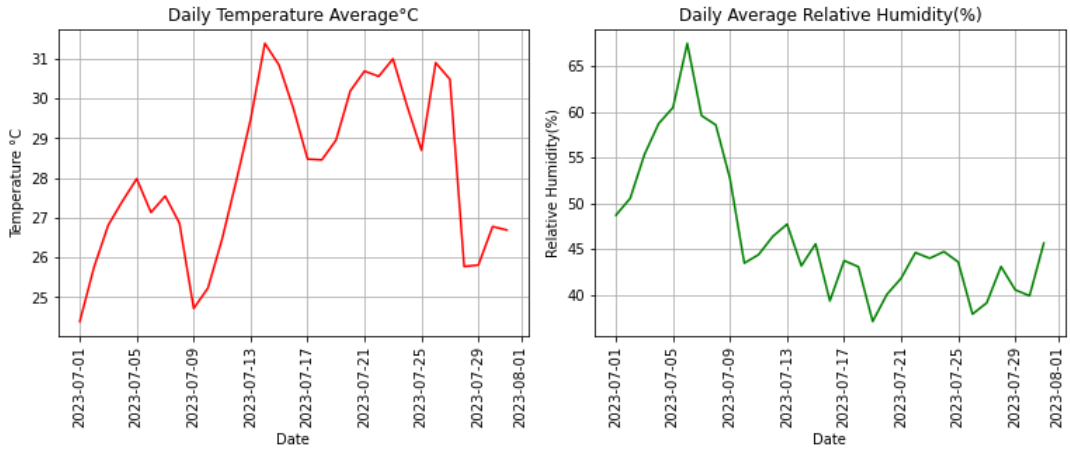

Figure 2.5 : Daily Average Temperature Values Derived From 68 Observation Stations For July (on the left), Daily Average Relative Humidity Values Derived From Observation Stations For July (on the right).

In this study it was decided to determine the days with daily average temperatures equal to or above the threshold value of 28°C. From the Figure 2.5, between the 13th of July and the 27th of July, daily average temperature values never dropped below 28°C; meanwhile, relative humidity values were below 45 % during the same period. According to State Meteorology observations, the highest temperature record belongs to the 26th of July, which is also one of the lowest relative humidity values during the case period for all the observation stations located over the selected domain.

To investigate the role of urbanization on record-breaking temperatures, the model runs between the 1st of July and the 31st of July as a case period due to the heatwave period, the 13th of July, and the 27th of July, which covers record-breaking days on the 26th of July.

2.4 Model Configuration

The Weather Research and Forecasting (WRF) Model developed by NCAR is a mesoscale numerical weather prediction model designed for atmospheric research and

operational forecasting needs (WRF model website, 2010). WRF model also provides an environment for various options suitable for case studies. In this study WRF model version 4.3 used to simulate urban heat island effect for determined case period and domain structure designed as nested 9, 3 and 1 km domain can be seen at Figure 2.6.

Model physic options selected based on previous study conducted for the same domain which are microphysics option as Lin et al., longwave radiation option as RRTM scheme, Dudhia scheme as shortwave radiation scheme, boundary-layer option as YSU scheme. In the study, when two different PBL options, YSU and ACM2, were tested, the lowest RMSE and MAE scores were obtained from the YSU runs. Furthermore, when the performance of YSU and microphysics options including Lin, Thompson, and WSM6 were analyzed, YSU and Lin exhibited the lowest error metrics. (Saka et al, 2021) Therefore, YSU and Lin combined parameter set configuration used for a monthly run, July 2023, and further details about the namelist of WRF can be found in Appendix A.

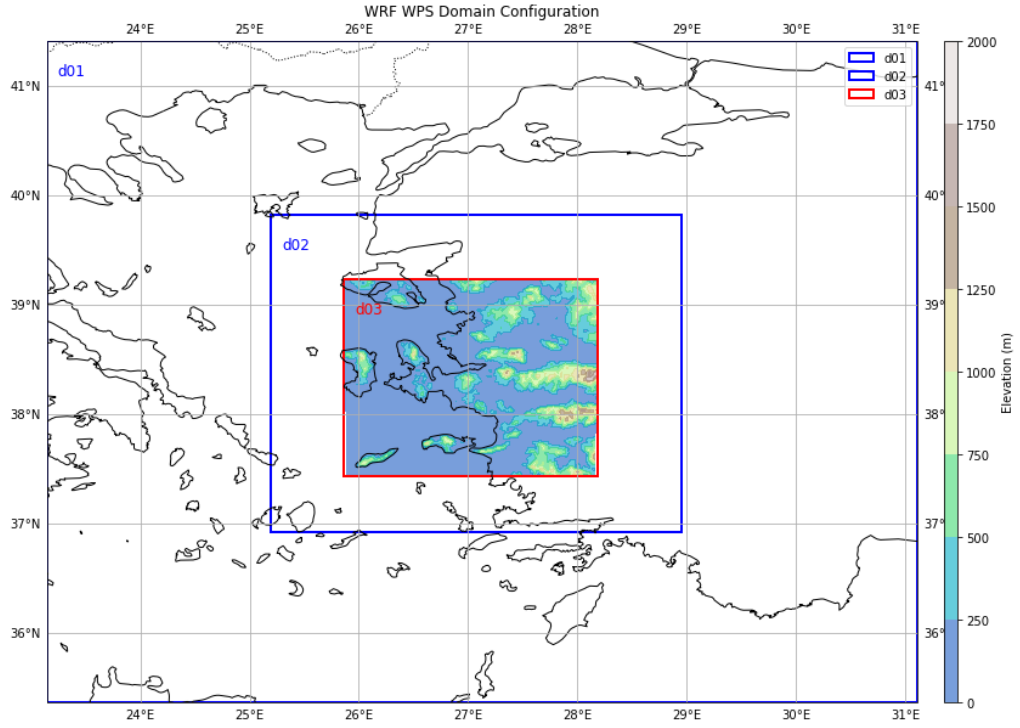

Figure 2.6 : Representation of nested domain configuration over selected domain.

Figure 2.7 a. represents how land cover varies over the selected domain and for further details about color representation of CORINE, please visit Appendix B. Figure 2.7 b. shows the land usage categories of the domain. In order to understand how urban areas affect atmospheric conditions, after the case period was decided, we converted the

urban land category to the closest rural category, which can be seen in Figure 2.7. This category change was made only for the third domain because the main urban area we wanted to focus on was represented within this domain.

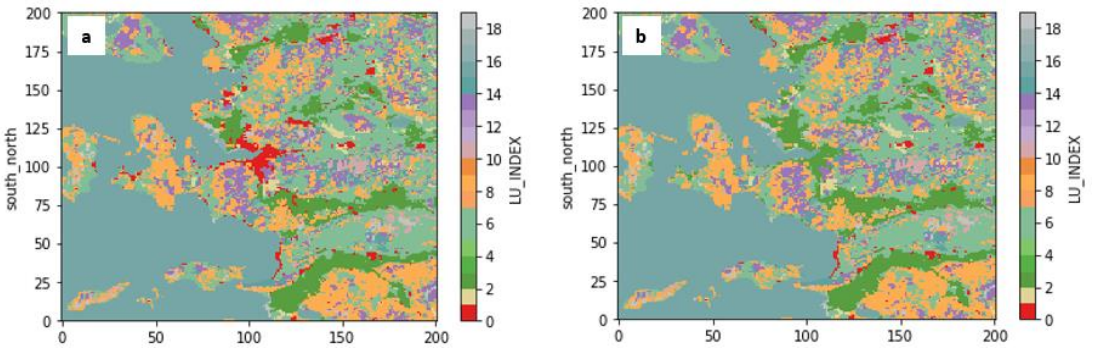

Figure 2.7 : CORINE landuse category change for domain.

2.5 Model Validation Metrics and Taylor Diagrams

There are many different statistical methods and formulas that can be used to measure model performance. In this study, we aimed to use the most representative and frequently used metrics for the model employed in the field of atmospheric sciences. Mean error, mean absolute error and root mean square error are the most common scale dependent metrics for model performance accuracy.(Hyndman and Koehler, 2006) so considering this information, in this study Root Mean Square Error and Mean Absolute Error metrics were selected for systematic performance evaluation.Root Mean Square Error (RMSE) is a widely used metric for evaluating the accuracy of a model. It measures the normalized average magnitude of the errors between predicted values and observed values. The formula for RMSE is given by:

$$RMSE = \sqrt{\frac{\sum_{i=1}^{n}(x_i - y_i)^2}{n}} \tag{2.1}$$

Another metric used to evaluate performance metric for this study is Mean Absolute Error (MAE) which gives average variance between observed and modeled values. The formula for MAE is given by:

$$MAE = \frac{\sum_{i=1}^{n}|x_i - y_i|}{n} \tag{2.2}$$

During this research,while searching for the optimum performance evaluation metric for this study, Taylor diagrams also standed out. Taylor diagram method is a graphical tool used in statistical analysis to succinctly summarize the relationship between

observed and modeled data, primarily in the fields of meteorology and climate science. This diagram provides a visual representation of three key statistical measures: the correlation coefficient, the standard deviation, and the centered root mean square error (RMSE) between the model predictions and the observations. By plotting these metrics in a single, two-dimensional graph, Taylor diagrams facilitate the evaluation of the accuracy and performance of different models. The radial distance from the origin represents the standard deviation, the angle from the horizontal axis indicates the correlation coefficient, and the distance from a reference point on the x-axis (usually representing the observations) corresponds to the centered RMSE. This comprehensive visualization allows researchers to quickly compare multiple models and identify which ones best replicate the observed data patterns, thereby aiding in model selection and improvement (Taylor, 2001).

3. RESULTS

The first part of this section evaluates the model's performance by comparing its outputs to the observed values over the entire month of July 2023. The comparison involves analyzing various performance metrics such as mean absolute error (MAE), root mean square error (RMSE), and correlation coefficient (r). These metrics provide a comprehensive assessment of the model's accuracy and reliability.. Then, the performance of the model within the selected heat wave case period are is particularly examined for its ability to capture rapid changes and anomalies. Finally, the study examines the changes observed when the urban categories in land use are replaced with the most dominant category around the urban araeas. This analysis helps in understanding the influence of urban areas on the key atmospheric variables influenced by the urban envirenment.

3.1 Model Validation

3.1.1 Performance metrics

The performance analysis began by evaluating the model's performance at the specific points designated for the Urban Heat Island Intensity calculation. The the Izmir Bolge Station was selected to represent the urbanized area, while the Seferihisar Station was selected to represent the rural area. RMSE and MAE scores were utilized for the point-based validation of this stud as these metrics provide a normalized assessment of model accuracy, facilitating comparison between different simulations and observations. Subsequently, the performance of the simulated atmospheric variables for urban and rural stations were calculated separately for the entire month and the selected case period. This approach allows for a detailed understanding of the model's performance over a longer timeframe as well as under specific heat wave conditions. The first provides a comprehensive view of the model's ability to predict the average urban heat island over İzmir, and helps in identifying the model's robustness. However, the second is important for assessing the model's responsiveness to rapid changes and extreme conditions. Table 3.1 shows the calculated error metrics for Monthly and Case

period performance for 2-meter Temperature values. The first two columns represent urban station results, while the other 2 represent the rural station results. The table 3.1 is structured to clearly differentiate the results for the urban and rural stations which gives insight into how well the model captures temperature variations in an urban and rural settings.

Table 3.1 : Evaluation metric results for urban and rural stations.

		URBAN STATION		RURAL STATION	
		NRMSE	NMAE	NRMSE	NMAE
Case	T2M	0.43	0.35	0.38	0.32
Month	T2M	0.18	0.15	0.38	0.32

When examining the performance metrics, during the case period, the model had lower error scores at the rural station than at the urban one. It suggests that the model is not adequetly capture the surface energy balance components and local circulation around the urban areas during the extreme heat wave episode. No significant performance changes were observed for the rural station between the case period and overall monthly scores, while the urban station model performed better for the month compared to the case period. In a WRF modeling study conducted in July 2009 on the urban heat island effect in Greece, it was found that the 2-meter temperature values in urbanized areas had an MAE of -0.58 and an RMSE of 1.35 when compared to observations. In the same study, the MAE for rural areas was calculated to be 0.55, while the RMSE was higher than that of urban areas, at 1.67 (Giannaros et al., 2013). This aligns with the values we have found. Another study using WRF for China reported that the MAE values for 2-meter temperature during the summer months ranged from 1.06 to 1.74 (Duan et al., 2018). When compared with studies in the literature that used similar areas and methods,and considering the error metrics threshold values, performance evaluation metrics at Table 1 shows an evident that the model demonstrates acceptable performance on a point basis.

3.1.2 Validation using Taylor diagrams

In order to evaluate model performance for representative stations for urban and rural characteristics, we chose the Taylor diagram method and calculated metrics based on data from urban and rural observation stations for the closest representing grid points from the WRF model outputs. Taylor diagrams are powerful tools for the statistical evaluation of model performance, offering a comprehensive visualization of how well

models simulate observed data by combining three crucial metrics: standard deviation, correlation coefficient, and centered root-mean-square error (RMSE).

Figure 3.1 shows the Taylor diagram created for the periodfrom the 1st of July to the 31st, comparing model temperatures with observed temperatures at the Izmir Bölge (urban station) and Seferihisar (rural station). Model performance for both urban and rural stations are similar in terms of standard deviation, indicating that the model captures the variability in temperature data consistently across different land cover types. Onthe other hand the rural stationdemonstrates a higher correlation compared to rural station, suggesting that the model's predictions are more closely aligned with the observed data in the rural area, reflecting a stronger linear relationship between model outputs and actual measurements .In addition, the rural station also shows lower RMSD scores than the urban stations during the month which can be attiributed to less severe discrepancies between predicted and observed temperatures compared to the urban station. . Overall, the model demonstrates acceptable performance for the month of July with a reasonable representation of temperature variations when compared to observations. The Taylor diagrams here effectively highlight the differences in model accuracy between urban and rural settings, underscoring the importance of considering land cover and local environmental characteristics in model evaluations.

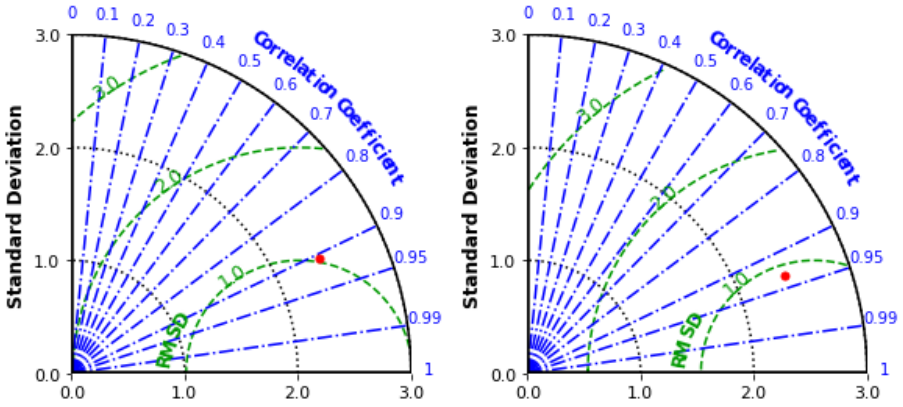

Figure 3.1 : For July 2023, İzmir Bölge station Taylor diagram on the left and Seferihisar station Taylor diagram on the right.

We also generated Taylor diagrams to evaluate how the model performed during the selected case period, which are illustarated in Figure 3.2 as a diagram for the urban station on the left and a diagram for the rural station on the right. When diagrams were examined, model performance for both point base stations, selected case period 13th-27th of July performance, was declinedcompared to the model performance for the

entire month. For both stations, the standard deviation of the models stayed around the same levels; however, correlation and RMSD scores dropped significantly during the case period. The model's ability to capture variability did not change significantly during the case period. However, the lower correlations and higher RMSD suggest that the model's estimations were less aligned with the observed data, reflecting a weaker linear relationship and larger discrepancies between the magnitudes of the estimated and observed temperatures. Similarly, the rural station also showed reduced performance with decreased correlation and increased RMSD eventhough the standard deviation remained stable.These comparisons suggests that the model representation of the dynamics of the urban environment iscompromised under the heat wave conditions.

These results identify specific weaknesses in the model that might not be as apparent during a longer simulation periods. This type of analysis is crucial for understanding the model performance and its reliability, particularly under varying extreme atmospheric conditions.

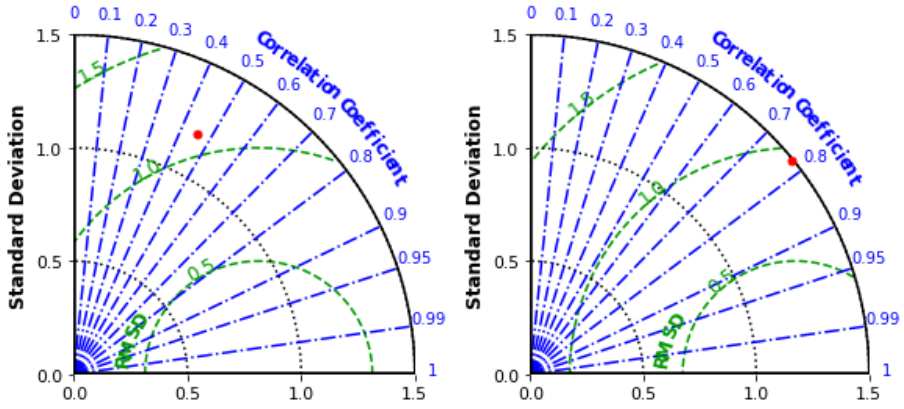

Figure 3.2 : For 13th -27th of July Taylor diagram for Izmir bolge (on the left), seferihisar (on the right).

3.1.3 Vertical temperature structure comparison

Not only did we evaluate how the model performed near surface by using surface observations, but we also assessed its performance in capturing the vertical distribution of temperature. Therefore, we compared skew-T diagrams obtained from the Wyoming University with vertical cross-sections generated by the model.

Figure 3.3 shows the vertical temperature profile in the atmosphere during the record-breaking temperature day. Skew t diagrams in Figure 2.7 start at 12 Z on the 26th of

July to 0 Z on the 28th of July. When we compare the dew point temperature and temperature values derived from the model with actual measurements, it is observed that the model's overall performance in the atmosphere's upper layers is generally acceptable. However, it progresses more smoothly compared to the measurements and closely follows a profile very similar to the measurements in almost every layer. It is observed that the model captures inversions in the temperature profile between 1000 mb and 900 mb, but it does not show the same level of sensitivity in dew point temperature's accuracy.

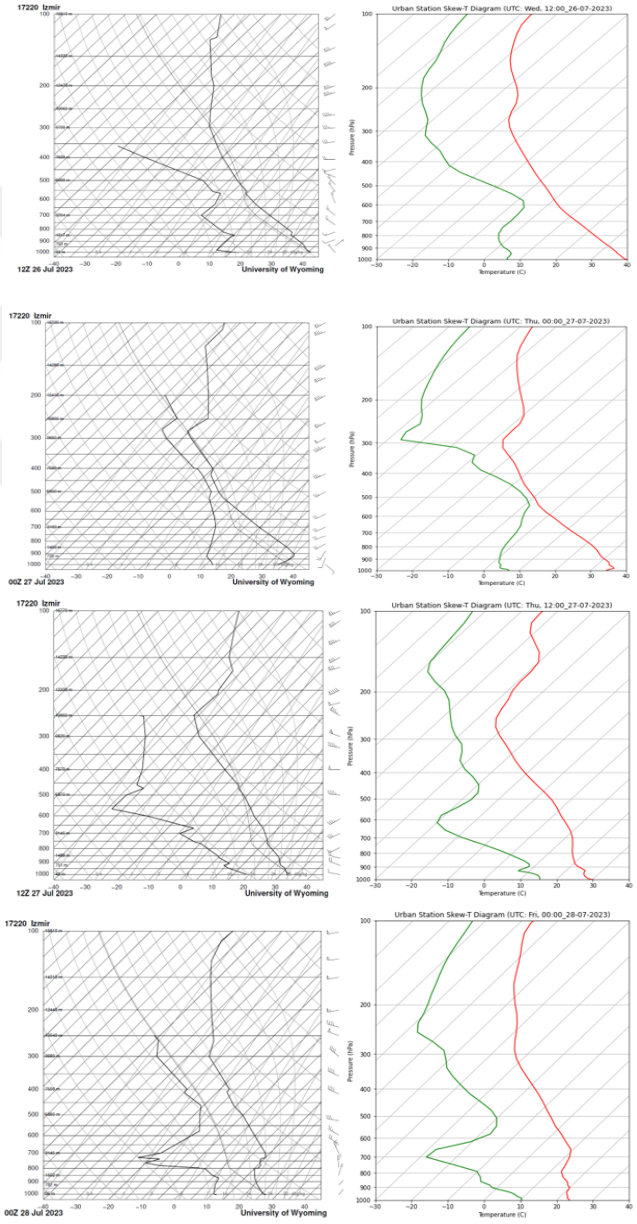

Figure 3.3 : Observed (left) and estimated (right) Skew-T Diagrams for Record Breaking Temperature Days of a) 12 Z, July 26, b) 00 Z, July 27, c) 12 Z, July 27, d) 00 Z, July 28.

3.1.4 Evolution of 2m temperature

The most fundamental meteorological parameter used to represent and calculate the urban heat island is the 2-meter temperature. When examining the hourly evolution of temperature distribution from the model, it is noted that the highest values in the urban area reached during the early hours of the heat wave day while lowest temperatures are in areas with higher elevations.Daily average 2 meter temperature values from urban run model output can be seen at Figure 3.4. When looking at the daily average temperature values, it is observed that the temperatures in and around the center of Izmir do not drop below 26 °C throughout the month of July.

To conduct a more detailed analysis of the conditions, we wanted to compare the average temperatures for Izmir in two different periods by taking into account the sunrise and sunset times each day. When examining Figure 3.5 for the period from sunrise to sunset, it is observed that the daily average temperatures are higher from the 2^{nd} to the 7^{th} and from the 19^{th} to the 28^{th} of the month compared to other days.

When examining nighttime temperatures from Figure 3.6 , it is observed that from the 1^{st} to the 7^{th} of the month, temperature values are high regardless of location and time. On the remaining days, areas with urban land use categories have higher temperature values compared to their surroundings.

.

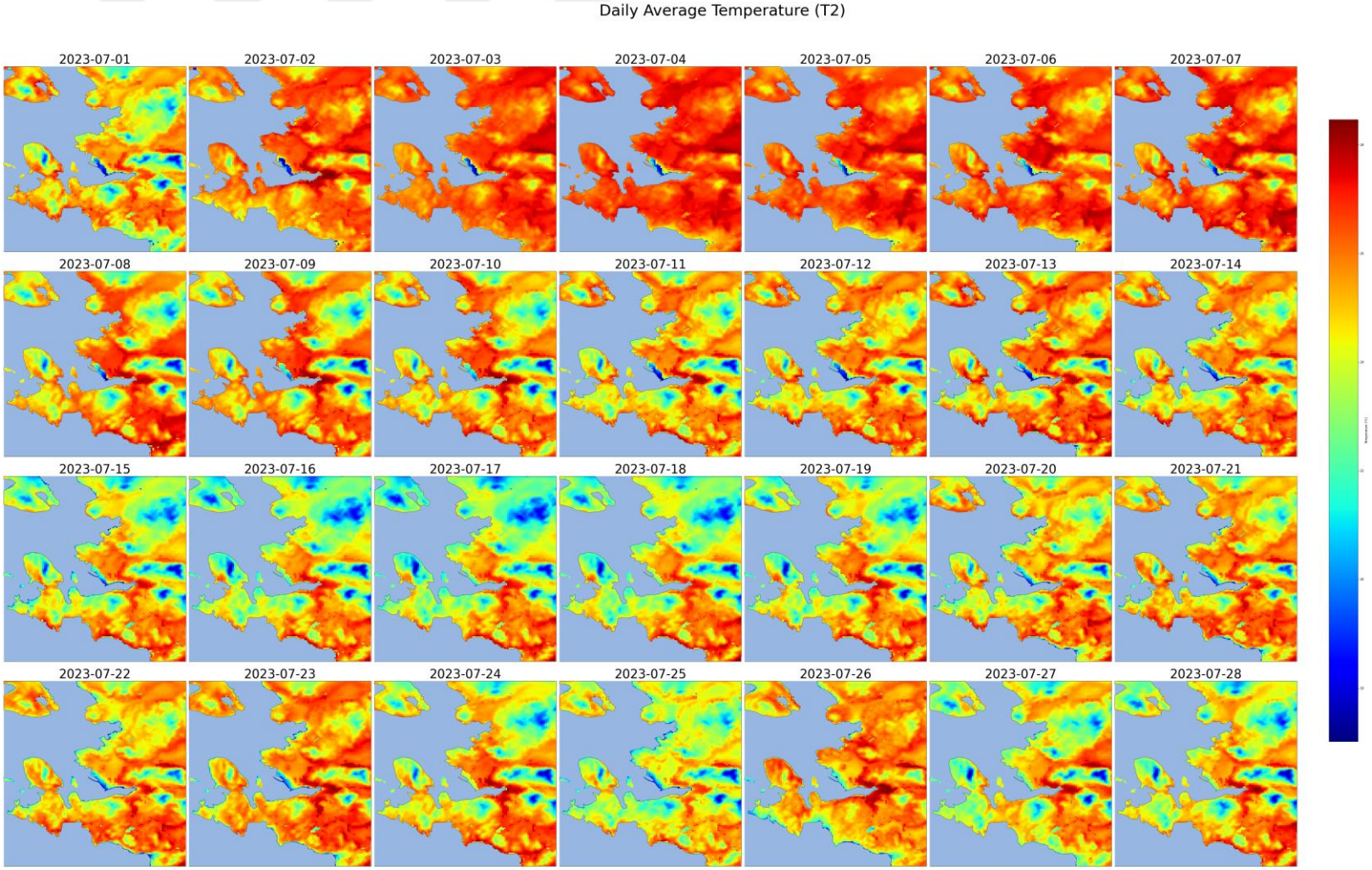

Figure 3.4 : Daily average temperature averages from urban run.

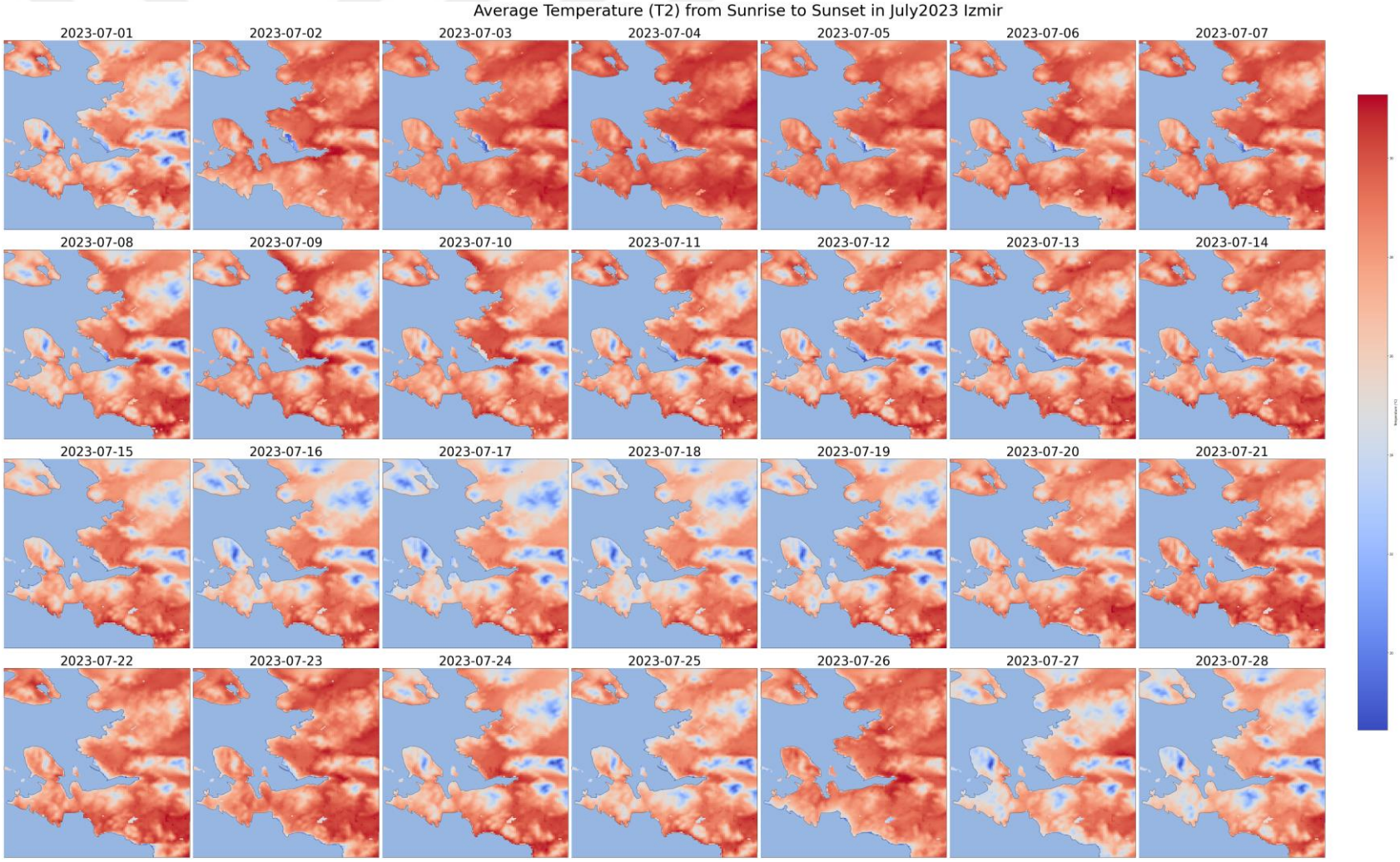

Figure 3.5 : Daily average temperature values from sunrise to sunset for July 2023.

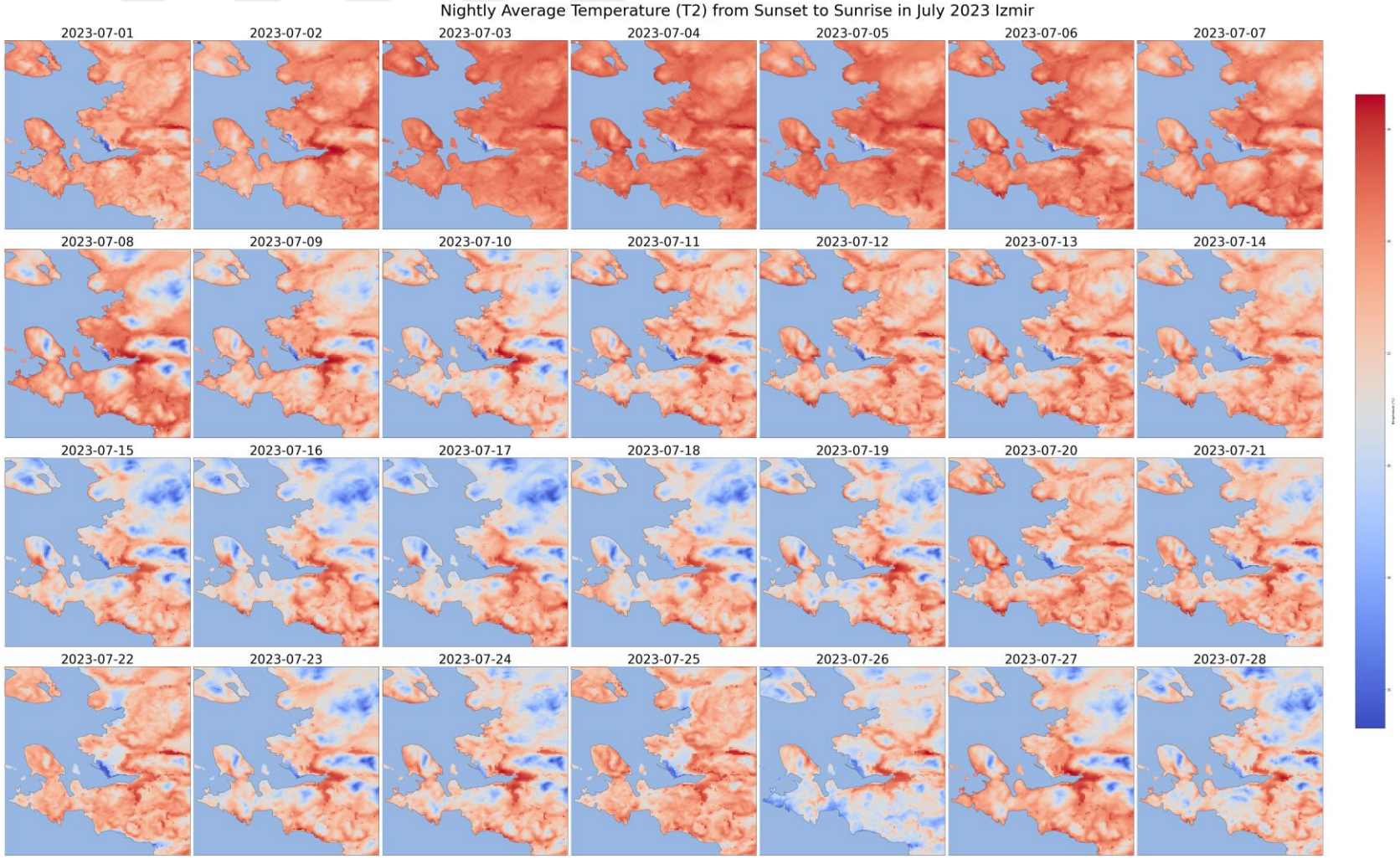

Figure 3.6 : Daily average temperature values from sunset to sunrise for july 2023

When examining the spatial distribution of temperature on the date when the record was broken at Figure 3.7, it is observed that the values started to increase six hours before the record-breaking temperatures were observed and then dropped more significantly on July 27 compared to the previous hours. When we evaluate the spatial distribution map together with the land use information mentioned in the previous sections, two details stand out. One is that the temperature varies as expected due to the topographic structure of the region, and the other is that the areas categorized as urban have higher temperature values compared to their surroundings as of midnight on July 27. This temperature difference between the urbanized area and its surroundings at night is defined as the nocturnal urban heat island (Oke, 1982) and can be clearly observed in Figure 3.7 during the evening hours before the temperature record was broken.

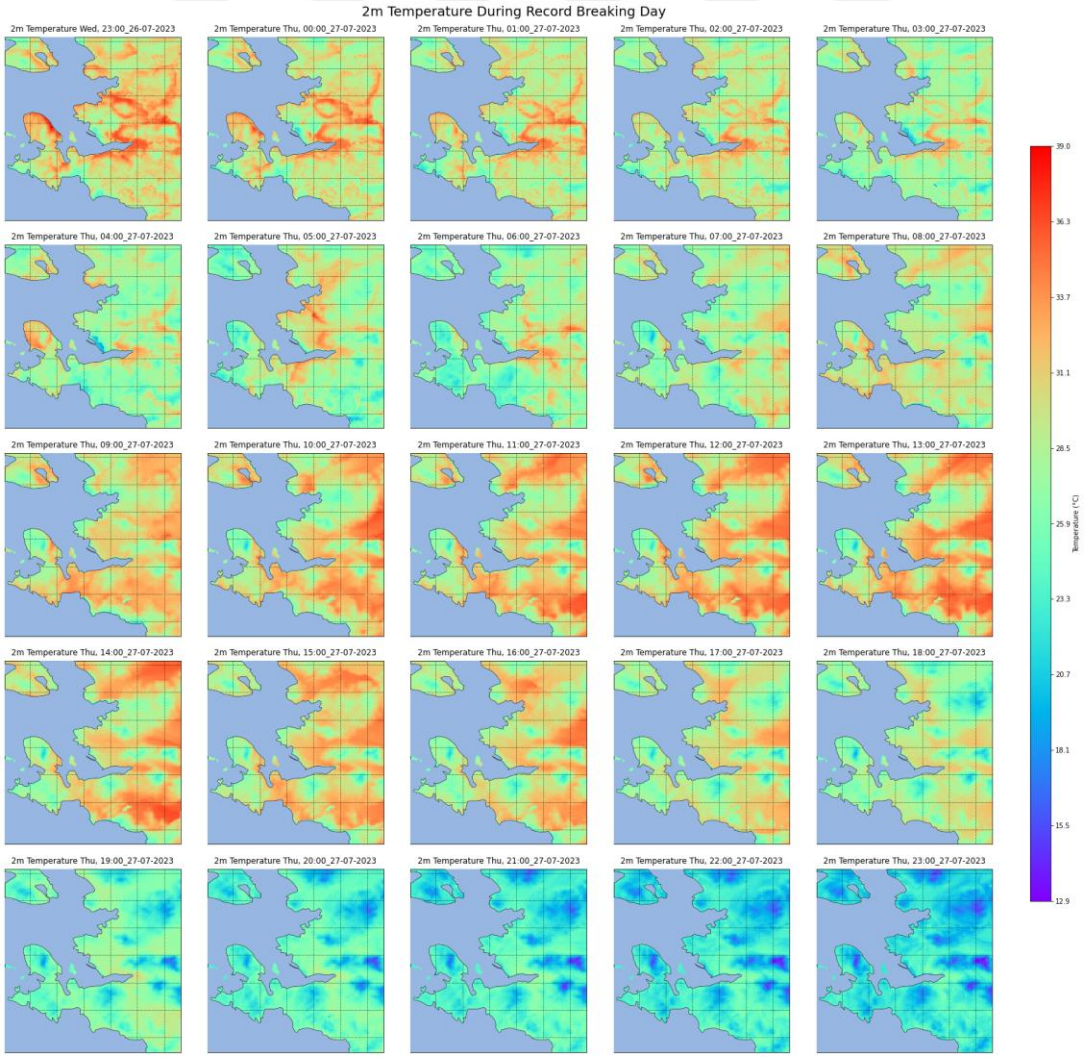

Figure 3.7 : 2m Temperature values from model output for record breaking day.

3.1.5 Evolution of boundary layer height

As detailed in the previous section, the atmospheric boundary layer is considered the lowest part of the atmosphere, and therefore it is influenced by temperature and wind changes as part of the surface energy balance (Oke, 1985). Considering that temperature is one of the main factors determining the boundary layer height, the temperature differences mentioned in the previous section are also expected to correlate with the boundary layer height. To verify this, the boundary layer values for the same period during which the temperature values were analyzed are plotted in Figure 3.8.

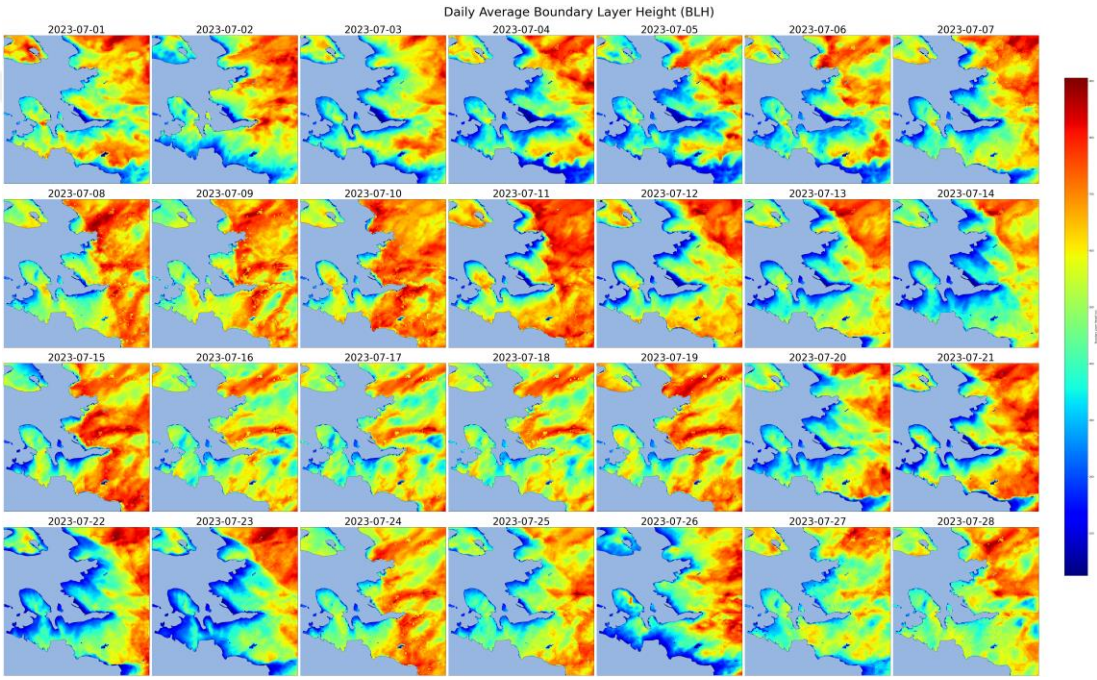

Figure 3.8 : Daily average boundary layer height from urban model run.

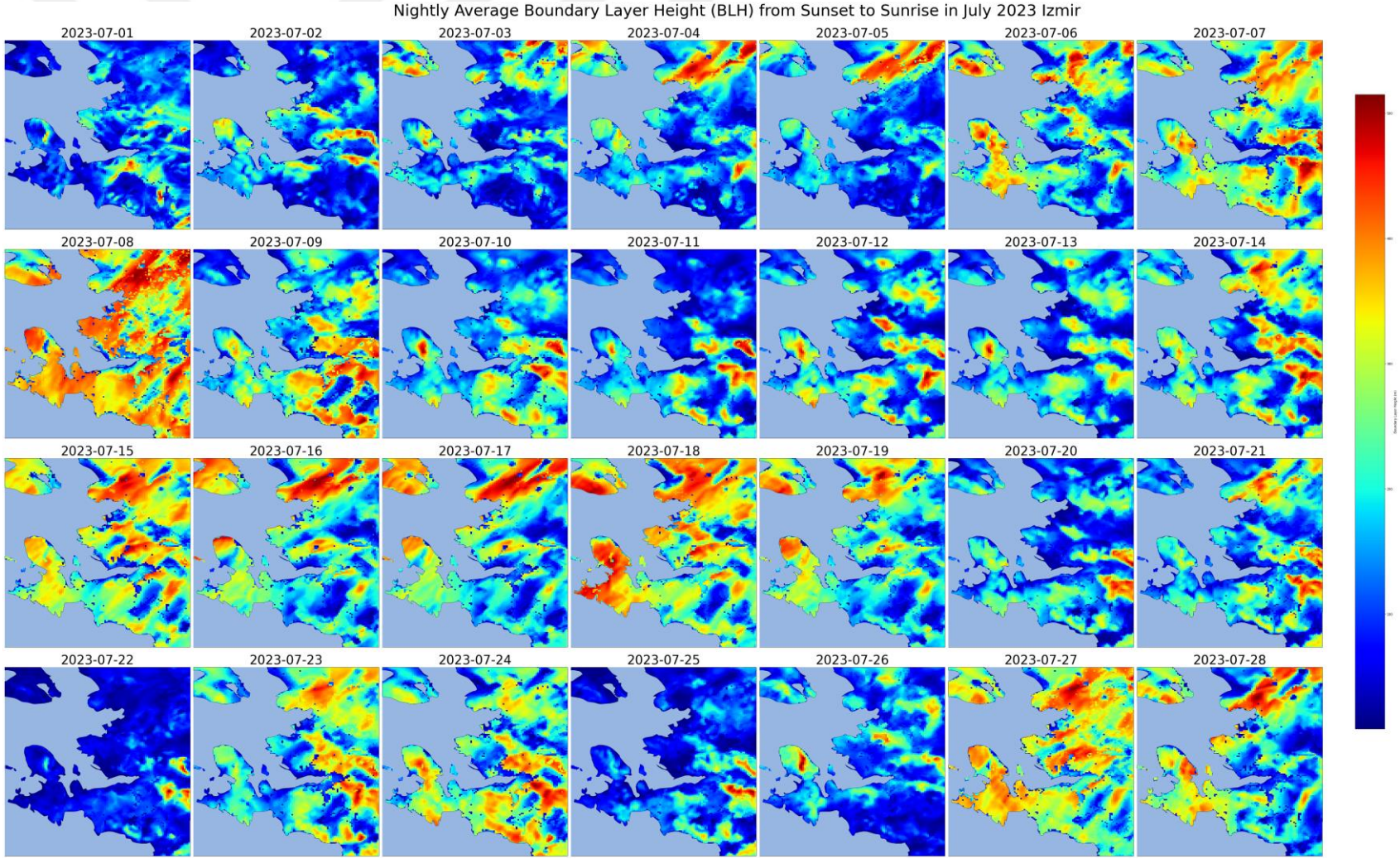

Figure 3.9 : Nightly average boundary layer height from sunset to sunrise.

3.1.6 Evolution of 10 m wind speed values

Wind speed and direction significantly impact boundary layer height and the urban heat island (UHI) effect. In urban areas, dense high-rise buildings often obstruct wind flow, leading to lower wind speeds which, in turn, result in reduced convective mixing within the boundary layer. This phenomenon exacerbates the UHI effect, particularly during heatwave events when the boundary layer height is lower, causing heat to be trapped near the surface. Studies in Beijing have shown that during heatwave periods, the intensity of the UHI effect increases as lower wind speeds prevent the dispersal of heat, leading to higher temperatures in urban areas compared to rural surroundings. Moreover, the heat retained in urban areas due to low wind speeds and high building density can elevate the UHI intensity by about 0.55°C during heatwaves compared to non-heatwave periods (Lian et al., 2021). Furthermore, the variability in boundary layer height is influenced by both local climate zones and atmospheric conditions. In rural areas, greater vegetation and water availability increase latent heat flux, while urban areas experience a rise in sensible heat flux, contributing to stronger UHI effects. During periods of low wind speeds, the disparity in temperature between urban and rural areas widens, further intensifying the UHI effect (Han et al., 2020; Lian et al., 2021). When the Figure 3.10 examined, it is observed that the wind speed is low in and around the city in July.

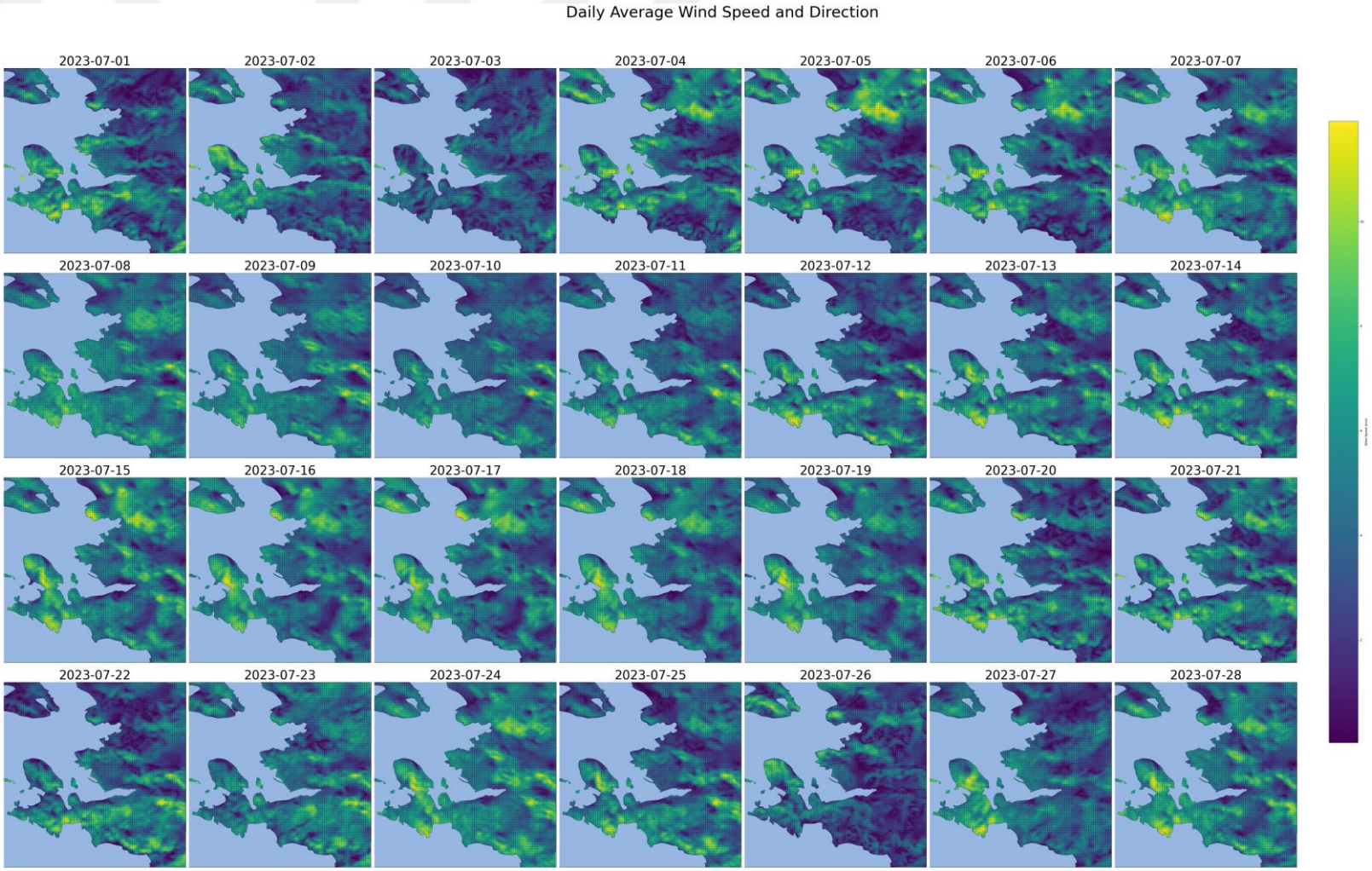

Figure 3.10 : Daily average wind speed and direction values from urban run.

3.2 Urban and Non-urban Run Comparison

In this study we removed the urban land category to determine the impact of the urban area. This section will discuss how meteorological conditions change when the urban effect dissapear.

3.2.1 Urban heat island intensity comparison

With the motivation of understanding how urban areas affect temperature values better, the temperature difference between rural and urban stations for both run outputs was calculated using Equation 1.1. Figure 3.11 shows the calculation of urban heat island intensity using selected urban and rural stations for urban and non-urban runs. Upon examining the analyzed results for one month, it is observed that the UHI intensity has decreased by approximately 1-1.5 °C . Additionally, the highest UHI intensity for both runs occurred on July 26-27.

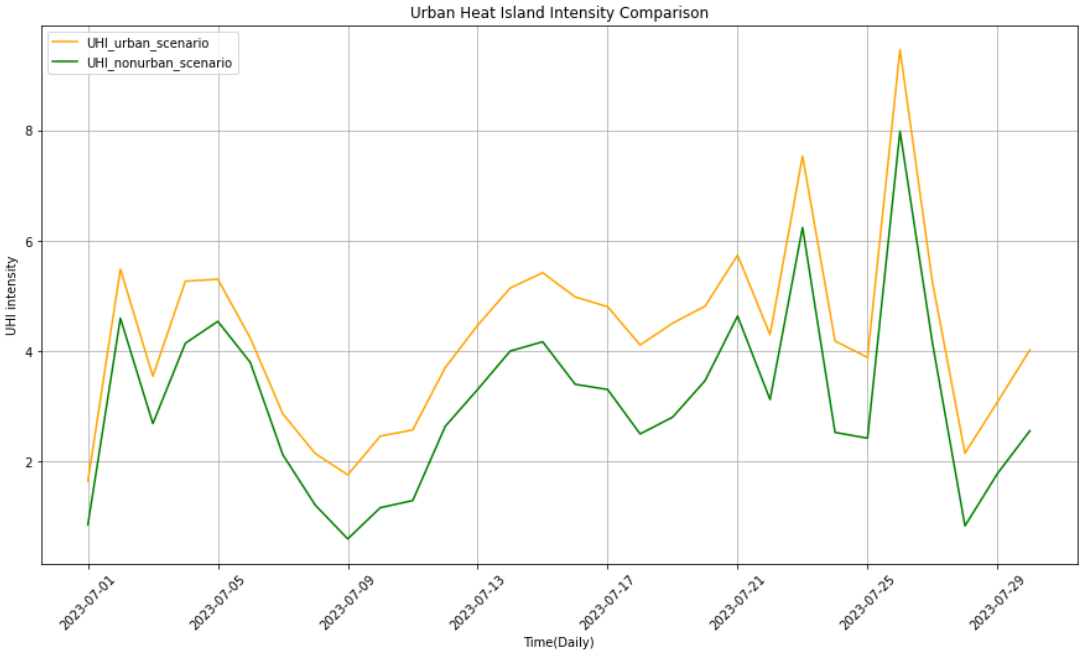

Figure 3.11 : Urban heat island intensity comparison between urban and non-urban runs for July 2023.

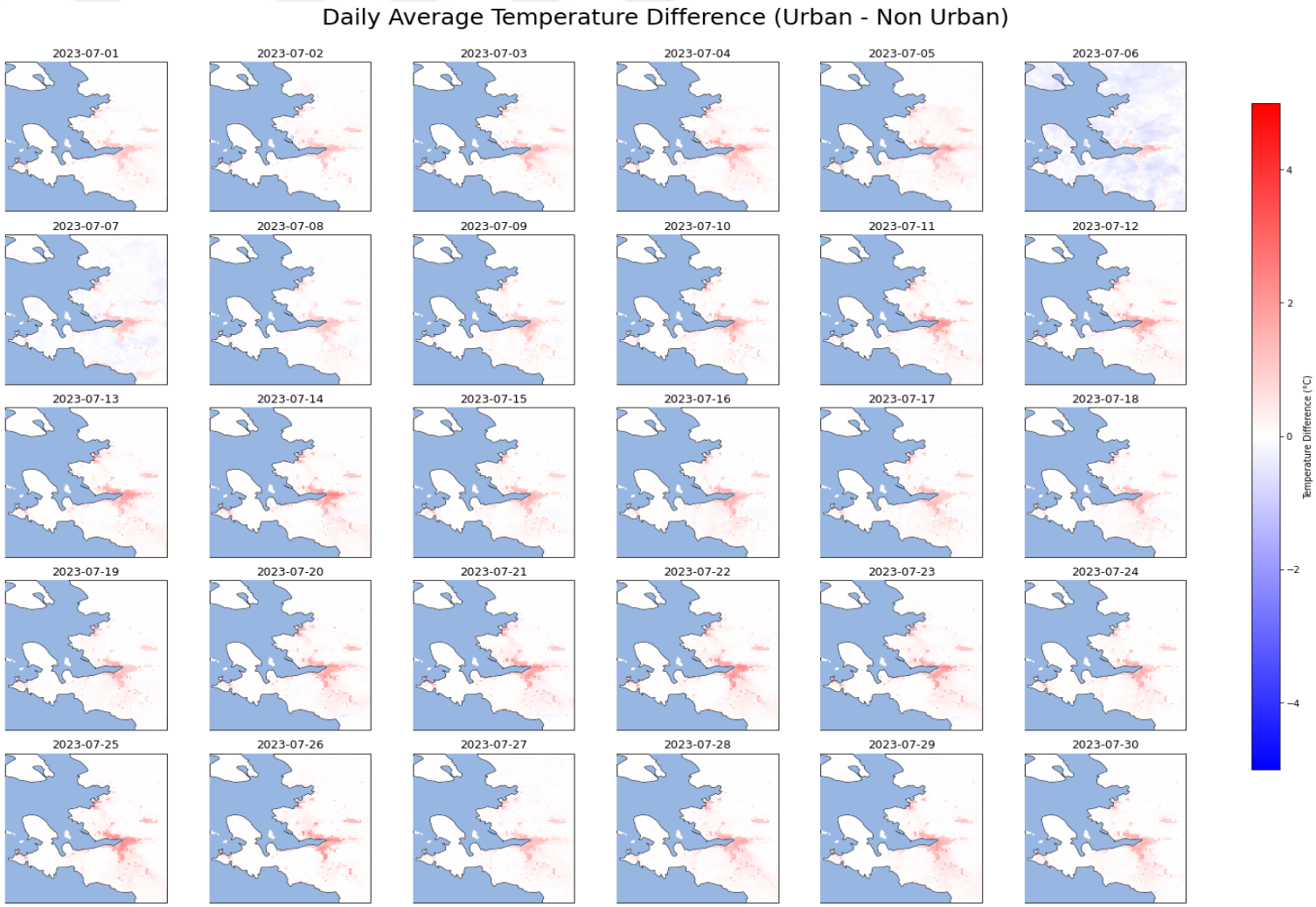

Figure 3.12 : Daily average temperature values between urban and non urban runs.

3.3 Heat wave Case Period Analysis

3.3.1 Evolution of boundary layer height for the heat wave period

Figure 3.13 shows the spatial variation of boundary layer height throughout the record-breaking day. The boundary layer values increase with sunrise and reach their highest levels a few hours after midday. Areas with high boundary layer values are associated with topography and urbanization ratio. The nocturnal variation observed in temperature values is also evident in the boundary layer values. However, unlike temperature, the boundary layer values observed during the day are relatively small.

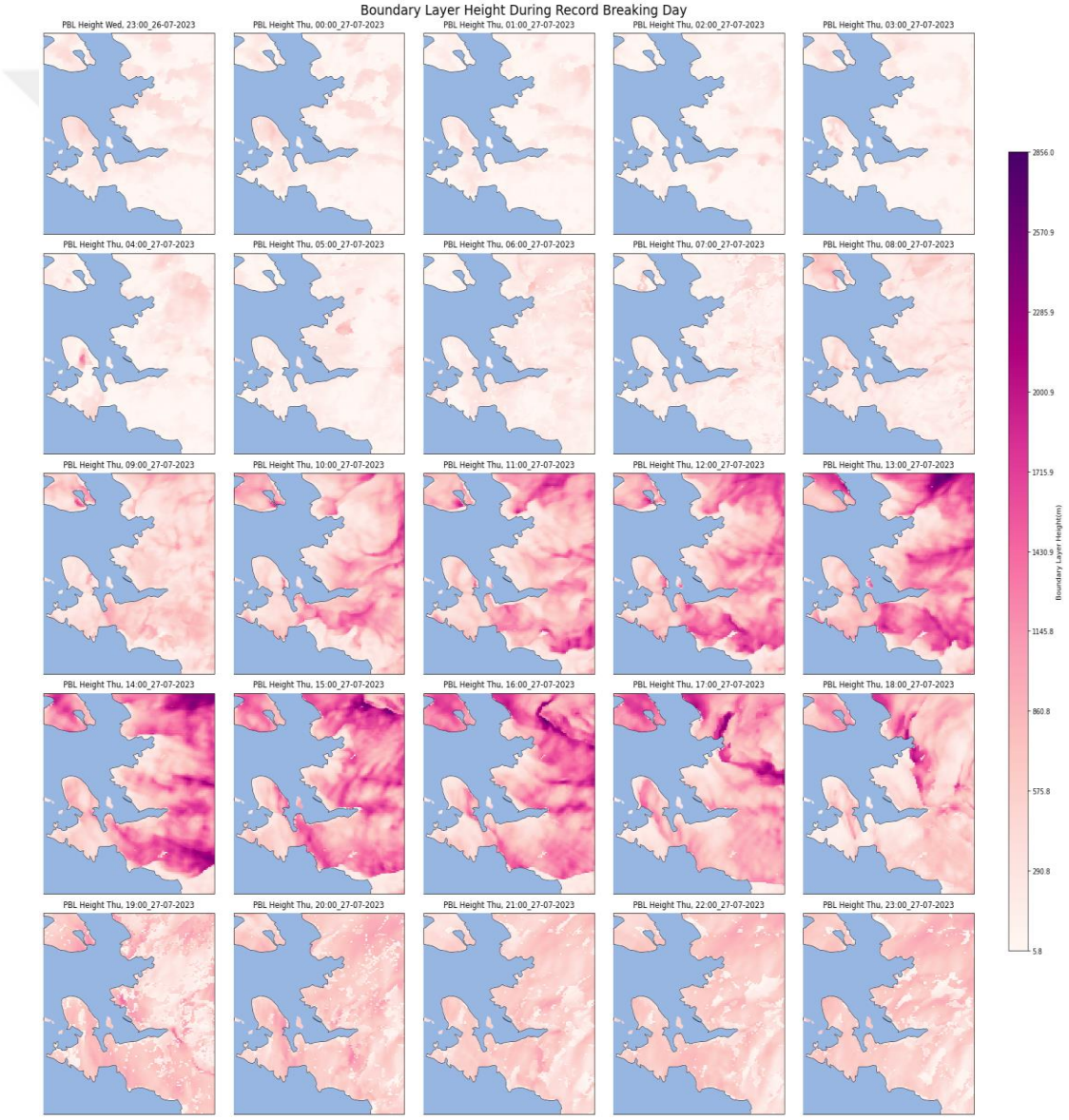

Figure 3.13 : Boundary layer height values from model output for record-breaking day.

3.3.2 Evolution of relative humidity for the heat wave period

The atmospheric humidity is expected to be low during a heatwave and under urban atmospheric conditions. Figure 3.14 shows the relative humidity values on the record-breaking day. As seen in the Figure, in the area with urban land use, the humidity level starts low in the early hours and does not exceed approximately 30% for several hours after the record temperature is reached.

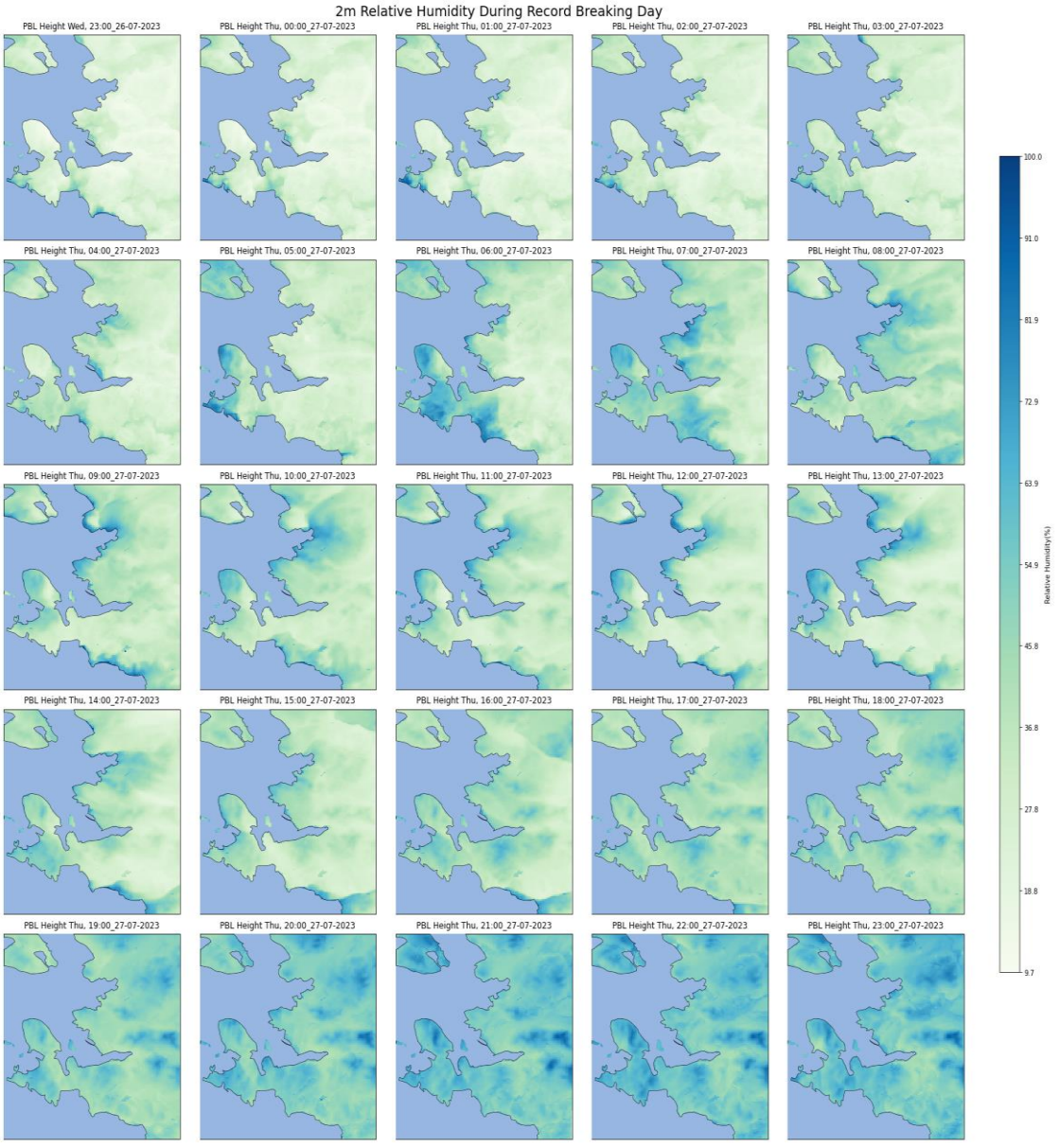

Figure 3.14 : Relative humidity values from model output for record-breaking day.

3.3.3 Evaluation of record breaking temperature day

As emphasized in other sections, the 2-meter temperature is the most fundamental parameter used in urban heat island calculations. When examining the temperature

differences between scenarios with and without a city, it has been observed that during the nighttime, when the urban heat island effect is expected to be most intense, the temperature values are higher when the city is present. Based on this, it is anticipated that the atmospheric boundary layer will be higher in the early hours of the day during a heatwave period when the city is present.

Figure 3.15 : Temperature difference across the area between the outputs of urban and non-urban model for the case period.

With changes in the urban structure, the humidity levels in the atmospheric layers are also expected to change. However, under the hot and dry conditions observed during the heatwave, it is understandable that there is no significant difference. Since the selected period is a hot, rain-dry, no significant differences in relative humidity values are observed between the two runs, apart from small local variations.

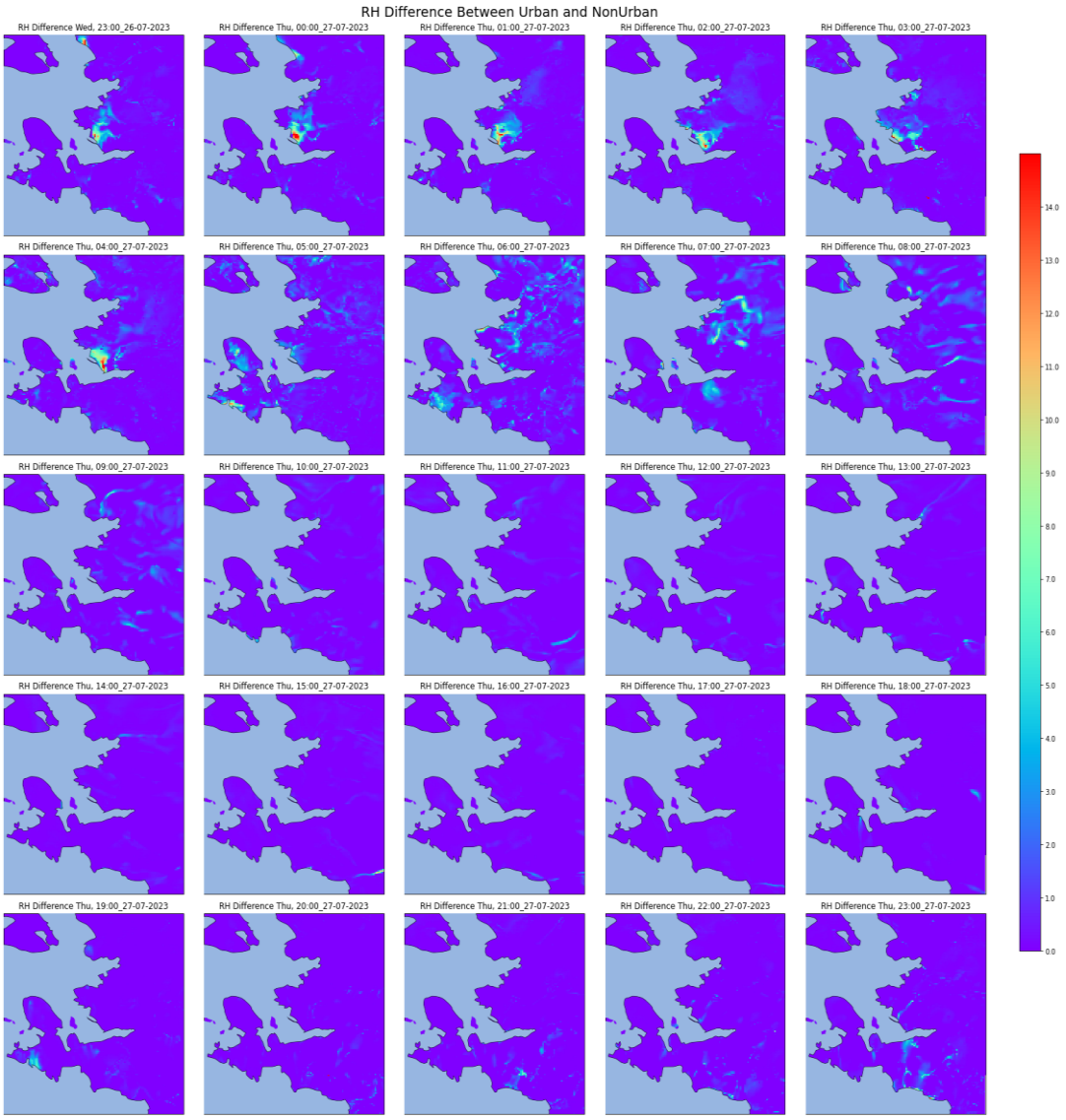

Figure 3.16 : Relative humidity difference across the area between the outputs of urban and non-urban model for the case period.

When urban structure changes, it is expected that boundary layer height will also change, as thermal equilibrium is altered. The changes in boundary layer values on the record-breaking day are shown in Figure 3.17. There was a noticeable difference in boundary layer height when comparing urban and non-urban simulations.

A close examination reveals that the boundary layer reaches its highest levels in the afternoon, driven by the intense solar heating and subsequent convective processes. Throughout the day, the boundary layer in urban areas exhibits more pronounced fluctuations. In the early morning, boundary layer is typically lower, but as the day progresses and the surface heats up, it rapidly expands. This expansion is more significant in urban areas due to the higher heat capacity of urban materials and also.

their higher surface temperatures as a result of the urban heat island (UHI) effect. Therefore, urban areas exhibit an elevated boundary layer compared to rural areas.

The presence of the city affects not only that area but also causes changes in the downwind regions controlled by topogtaphy as well The thermal gradients created by urban areas can modify the temperature profile of downwind regions, potentially leading to microclimatic changes.The simulation results suggest that the elevated boundary layer over urban areas can extend and modify atmospheric conditions far beyond the city's limits, affecting weather patterns and air quality in surrounding regions. The increased boundary layer height in urban areas can enhance vertical mixing so that more frequent and intense convective activities such as thunderstorms become more probable. In addition, these changes can also alter local wind patterns and potentially influence the development and movement of weather systems.

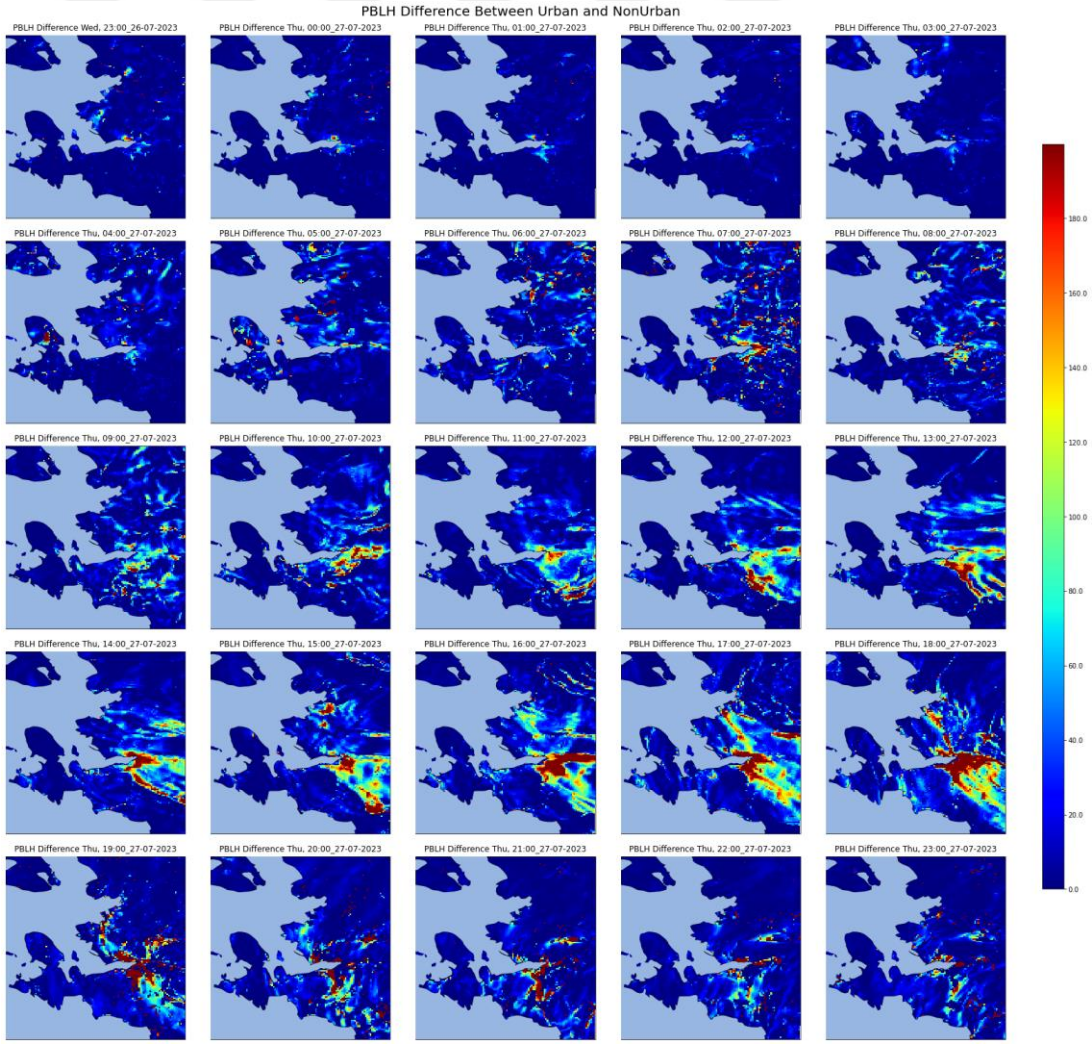

Figure 3.17 : Boundary layer height difference across the area between the urban and non-urban model outputs for the case period.

3.4 Analysis of Nocturnal and Diurnal Boundary Layer Heights During The Case Period

The nocturnal and diurnal boundary layer heights are crucial aspects of boundary layer meteorology, as highlighted by Oke (1985). During the daytime, the diurnal boundary layer typically develops due to solar heating, causing convective turbulence and leading to a well-mixed layer that can reach considerable heights. This layer is characterized by vigorous mixing and significant vertical motions. Conversely, at night, the absence of solar heating leads to the formation of a stable nocturnal boundary layer. This layer is often shallower and more stratified, resulting in reduced turbulence and limited vertical mixing. The nocturnal boundary layer can be influenced by various factors, such as surface cooling rates and terrain characteristics, which can lead to the development of temperature inversions and drainage flows that further stabilize the boundary layer (Oke, 1985; Godowitch et al., 1985). After the urban area was removed, the boundary layer heights during day and night at the point represented by the urban station were examined (Figures 3.18 and 3.19). No change was observed in the daytime boundary layer heights between the two runs. However, during the night, it was observed that the boundary layer height decreased when the urban area was absent. Since urban areas often experience higher temperatures at night compared to rural areas due to the heat retained by urban surfaces (asphalt, buildings etc.) and the reduced radiative cooling in cities, the nocturnal boundary layer becomes shallower compared to rural areas. The warmer urban surface reduces the temperature gradient between the surface and the overlying atmosphere, leading to a less pronounced vertical mixing. The heat absorbed in urban surfaces can keep temperatures higher for longer periods into the night and reduces the typical nocturnal cooling in rural areas. In addition, humidity levels at night in urban areas can be higher because of the factors like increased moisture from human activities, vegetation, and reduced ventilation. This can affect local dew point temperatures and contribute to higher humidity in the atmospheric boundary layer.

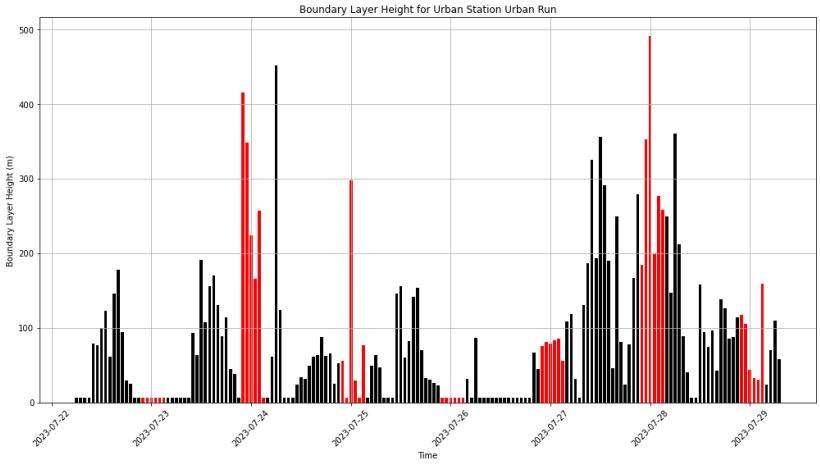

Figure 3.18 : Boundary layer height for urban station during heat wave period from urban run.

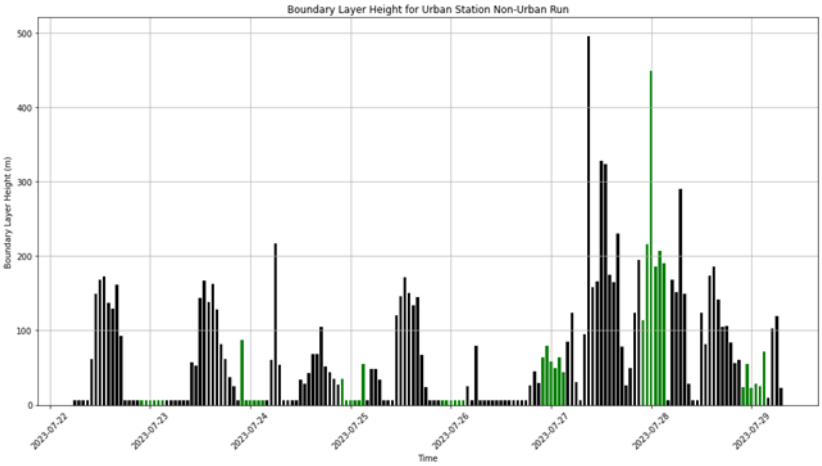

Figure 3.19 : Boundary layer height for urban station during heat wave period from non urban run.

3.5 Vertical Temperature Profile Comparison

One of the primary effects of UHI on vertical temperature distribution is the formation of a warmer air layer near the surface, which can extend upwards and affect the temperature profile of the urban boundary layer. This layer of warm air can be more pronounced during the day due to the absorption of solar radiation by urban surfaces, and it often persists into the night, leading to higher nocturnal temperatures compared to rural areas (Kaloustian & Bechtel, 2016; Martilli et al., 2020; Stewart et al., 2014). The vertical temperature profiles for both scenarios were plotted on the same graph and analyzed in detail. Figure 3.20 shows how these profiles change over time. Analyzing the dew point temperature and temperature values at 12-hour intervals before and after the heat wave episode for both scenarios reveals no differences

between the 200 hPa and 700 hPa levels at any time step. However, there are differences in dew point temperatures between the 700 hPa and 900 hPa levels at certain time points.

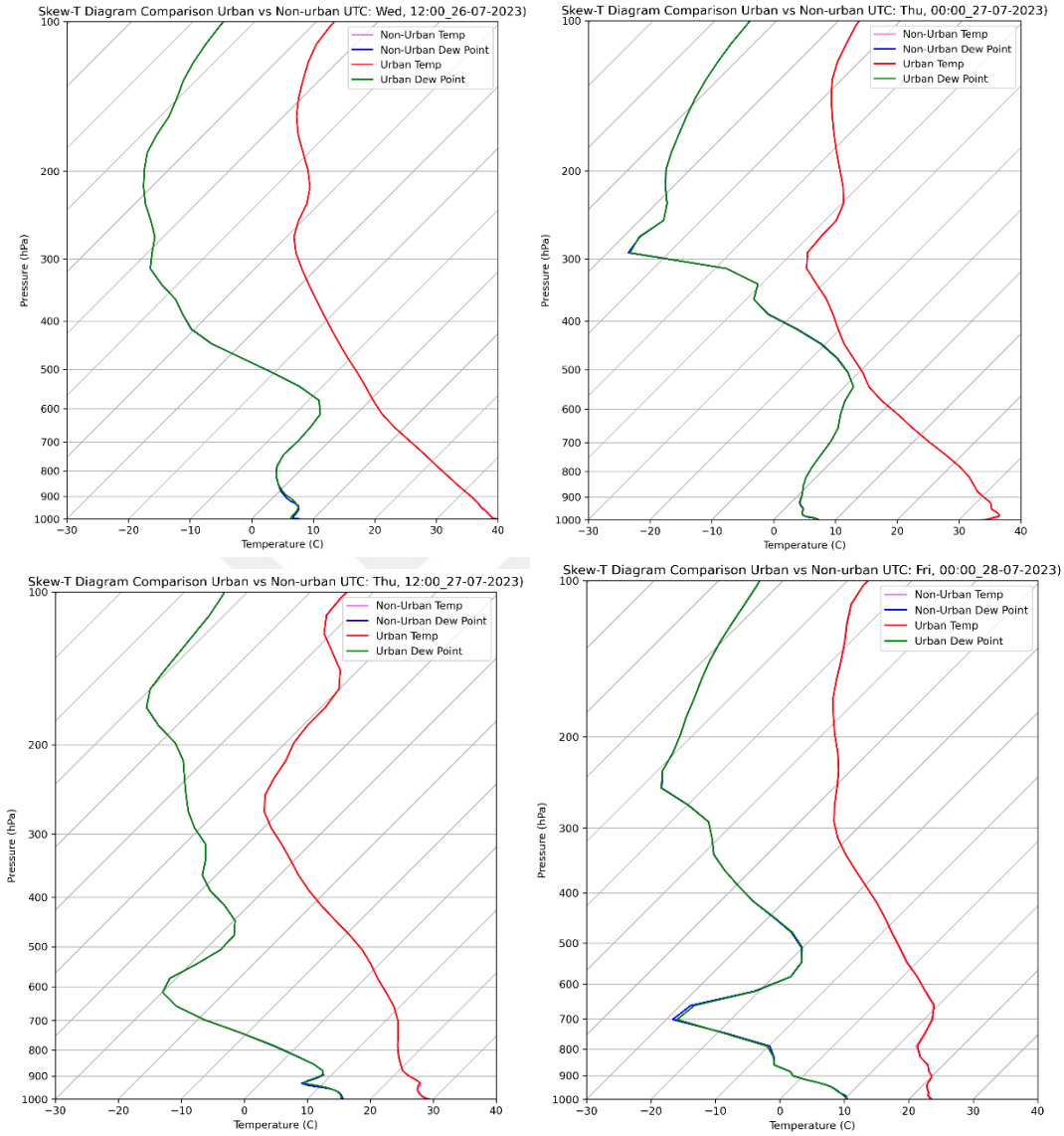

Figure 3.20 : Vertical temperature profile comparison for Urban and Non-urban run during record breaking temperature day.

Figure 3.21 provides a close-up view of the differences observed at the 700-900 hPa levels. Upon examining these graphs, it is evident that differences are seen between the 1000 hPa and 800 hPa levels before the record is broken, whereas after the record is broken, the differences are observed at higher levels.

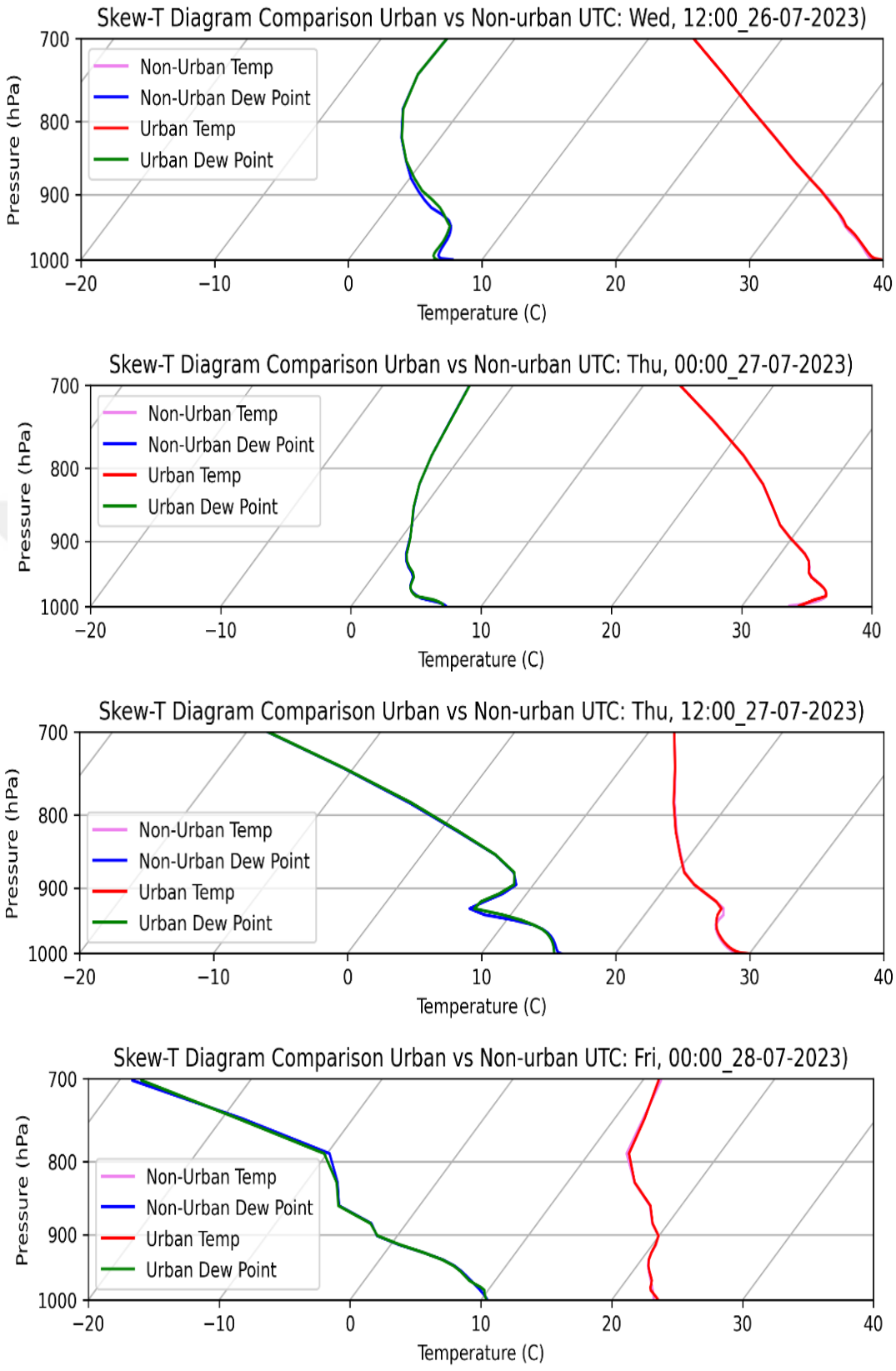

Figure 3.21 : Zoomed skewt diagrams for changing levels of the atmosphere.

3.6 Cross-section analysis for buoyancy flux

Urbanization significantly impacts buoyancy fluxes in the atmosphere. Urban areas, characterized by extensive concrete and asphalt surfaces, absorb and retain more heat compared to rural areas, leading to higher surface temperatures. This increased retention of heat, urban heat island effect enhances buoyancy fluxes and leading convection by modifying the lapse rate between the urban surface and the overlying air. Consequently, urban areas often experience stronger and more frequent convective activities, such as thunderstorms, compared to their rural counterparts (Oke, 1982). Additionally, the complex structures and varied surfaces in urban environments further influence airflow patterns and turbulence, significantly affecting buoyancy flux and local weather conditions (Grimmond & Oke, 1999). Buildings and other man-made surface materials can alter wind flow due to the drag, and create microclimates within the urban area which differ markedly from surrounding rural regions. Eventuaaly the increased mechanical turbulence, combined with thermal turbulence due to the UHI effect, results in unique atmospheric dynamics over urban areas and and change the horizontal temperature gradient between urban and rural areas. To quantitatively analyze the impact of urbanization on buoyancy flux, we calculated buoyancy fluxes using Equation 1.2 from the model outputs for both urban and non-urban simulations. These calculations are visualized in cross-sections shown in Figure 3.22. The urban area located in the cross section is located between coordinates 38°40'27.00″ to 38°42' 27.23″.

Buoyancy flux cross section for 26th of July at 12 Z, can be seen at Figure 3.22, when the land category changed to non-urban, it was observed that there were more descending movements over the urban area's location after local time mid-day. Meanwhile when the urban category was removed, it was observed that there was not a decrease, but rather an increase in upward movements in the atmosphere. This could be due to topography or the sea-land breeze effect.

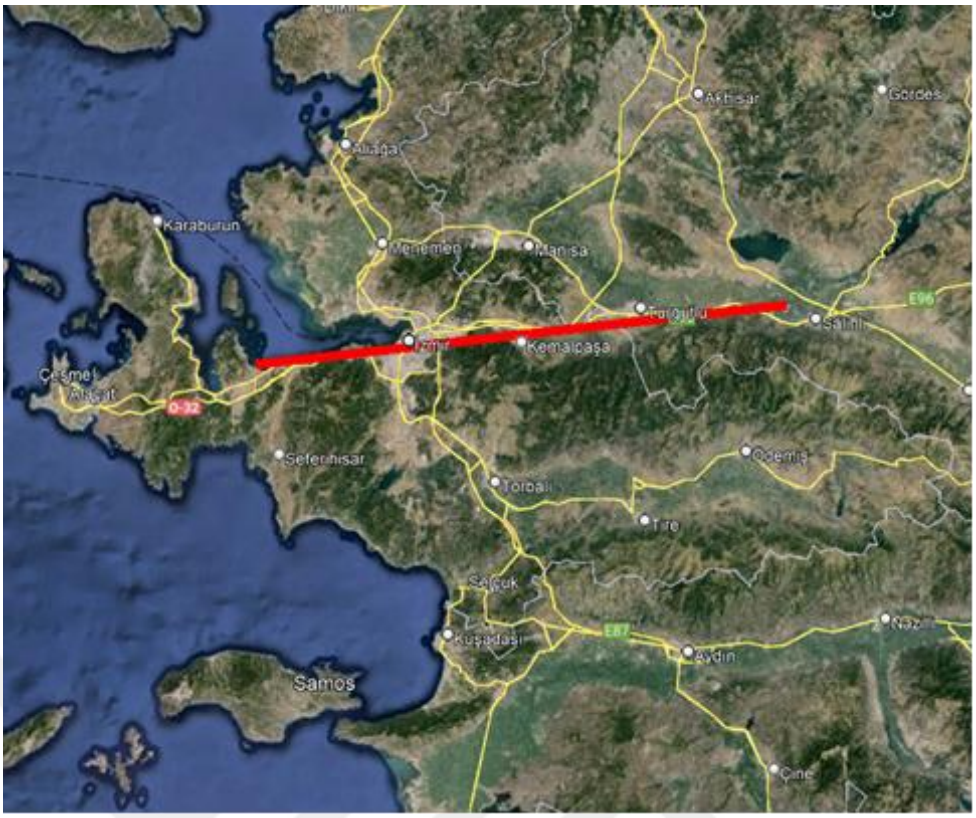

Figure 3.22 : Selected Vertical Cross-section path over the domain.

During the day time, temperature differences between the cooler sea and the warmer land drive the sea-breeze circulation. Sea breeze and urban local circulation can counteract each other in complex ways, particularly in coastal urban areas. The sea breeze brings in cooler air from the sea, which can lower temperatures in coastal urban areas. On the other hand, the urban heat island effect causes higher temperatures in cities, creating a strong thermal gradient between the city and its surroundings. The sea breeze moves inland, potentially opposing the outflow of warm air from the city. Warm air rising over the urban area can draw in air from the surrounding rural areas, including from the direction of the sea. The inflow of cooler sea breeze air and the outflow of warm urban air can create convergence zones. This can lead to enhanced upward motion, increasing cloud formation and sometimes convective precipitation. At the same time, the sea breeze can disrupt the urban heat island circulation by bringing in cooler air, which reduces the temperature difference and weakens the UHI-induced circulation. Off course, the actual result of the interaction between sea breeze and urban local circulation depends on various factors, including the strength and direction of the sea breeze, the intensity of the urban heat island effect, and local geographical features. Therefore, further investigation is needed to explore this

phenomenon in detail. Understanding these interactions might be important for urban planning and weather prediction, especially in coastal cities where these phenomena are pronounced.

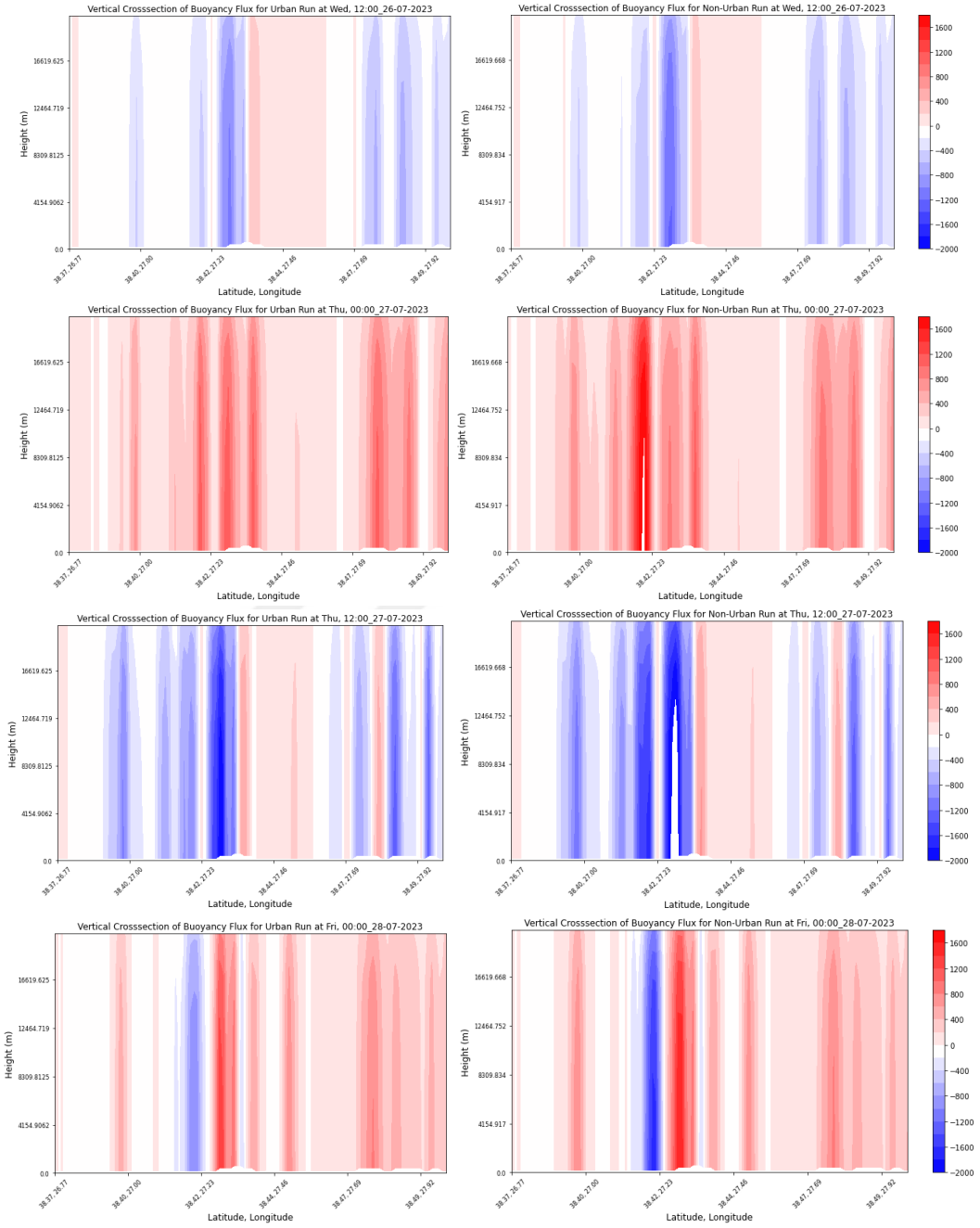

Figure 3.23 : Buoyancy Flux Cross-section for Record Breaking Temperature Days of Urban (left) and Non-urban (right) simulations of a) 12 Z, July 26, b) 00 Z, July 27, c) 12 Z, July 27, d) 00 Z, July 28.

4. CONCLUSION

This study aims to assess the effects of the urban heat island intensity on the boundary layer and temperature structure over İzmir, Türkiye, specifically on days with record-breaking temperatures. To conduct this study, we utilized the WRF model version 4.3. After establishing the necessary infrastructure and configuring the model, we investigated the appropriate parameter set. We chose the parameterization that most accurately represents the region based on previous research in the same field.

A crucial aspect of the study was incorporating land use data that reflects urbanization. Instead of default land use data, we used CORINE data to define the model's land use categories. Then, we conduct the simulations using the atmospheric model forced with ECMWF reanalysis data and selected the case date determined based on heat wave period in the observations. Subsequently, we obtained the simulations for July 2023, including the record-breaking day.

- The study revealed that replacing urban areas with rural land use significantly altered the area's temperature throughout the month. Notably, the minimum temperature difference between urban and rural areas during the record-breaking temperature day occurred at night, consistent with the urban heat island effect.
- There was an noticeable difference in boundary layer height when comparing urban and non-urban simulations. This difference is crucial for understanding how urbanization affects atmospheric dynamics.
- On a record-breaking day, the buoyancy flux was higher for the urban run during the day and lower at night, indicating complex interactions between urban heat and atmospheric processes, warranting further investigation to understand the underlying mechanisms fully.

Overall, this study provides important insights into the impact of urbanization on local climate conditions, particularly under extreme heat wave events. By using high-resolution land use data and detailed atmospheric modeling, we have highlighted

significant differences in temperature and boundary layer characteristics between urban and rural areas, emphasizing the importance of accurate urban representation in climate models.

REFERENCES

Anderson, G. B., & Bell, M. L. (2011). Heat waves in the United States: Mortality risk during heat waves and effect modification by heat wave characteristics in 43 US communities. Environmental Health Perspectives, 119(2), 210-218.

Bilang, R. G. J. P., Blanco, A. C., Santos, J. A. S., & Olaguera, L. M. P. (2024). Evaluation of WRF Model with Urban Canopy Models in Simulating Heat Events in Metro Manila. *Theoretical and Applied Climatology*.

Bossard, M., Feranec, J., & Otahel, J. (2000). CORINE land cover technical guide – Addendum 2000. European Environment Agency.

Büttner, G., Feranec, J., Jaffrain, G., Mari, L., Maucha, G., & Soukup, T. (2004). The CORINE land cover 2000 project. EARSeL eProceedings, 3(3), 331-346.

Chen, K., Boomsma, J. & Holmes, H.A. (2023) A multiscale analysis of heatwaves and urban heat islands in the western U.S. during the summer of 2021. Sci Rep 13, 9570 (2023). https://doi.org/10.1038/s41598-023-35621-7

Chen, F., Kusaka, H., Bornstein, R., Ching, J., Grimmond, C. S. B., Grossman-Clarke, S., ... & Taha, H. (2018). The Integrated WRF/Urban Modelling System: Development, Evaluation, and Applications to Urban Environmental Problems. International Journal of Climatology, 38(7), 2839-2849.

Chew, L. W., Liu, X., Li, X.-X., & Norford, L. K. (2023). Interaction between heat wave and urban heat island: A case study in a tropical coastal city, Singapore. *Journal of Climate Research*, *43*(5), 789-804. https://doi.org/10.1175/JCLI-D-22-0123.1

Chang Shu, Abhishek Gaur, Liangzhu Wang, Michael A. Lacasse, (2023) Evolution of the local climate in Montreal and Ottawa before, during and after a heatwave and the effects on urban heat islands,Science of The Total Environment,Volume 890,2023,164497, ISSN 0048-9697,https://doi.org/10.1016/j.scitotenv.2023.164497.

Garratt, J. R. (1992). The Atmospheric Boundary Layer. Cambridge University Press.

Grimmond, S., & Oke, T. (1999). Heat storage in urban areas: local-scale observations and evaluation of a simple model. Journal of Applied Meteorology and Climatology, 38(7), 922-940.

Garuma G.F. (2022). How the Interaction of Heatwaves and Urban Heat Islands Amplify Urban Warming. *Adv Environ Eng Res* **2022**; 3(2): 022; doi:10.21926/aeer.2202022.

Godowitch, J. M., Ching, J. K. S., & Clarke, J. F. (1985). Evolution of the nocturnal inversion layer at an urban and nonurban location. *Journal of Climate and Applied Meteorology*, 24, 791-804.

Hsiang, S., Kopp, R. E., Jina, A. S., Rising, J., Delgado, M., Mohan, S., ... & Mastrandrea, M. D. (2017). Estimating economic damage from climate change in the United States. Science, 356(6345), 1362-1369.

Howard, L. (1833). The Climate of London. John Murray.

Klein Rosenthal, J., Kinney, P. L., & Metzger, K. B. (2014). Intra-urban vulnerability to heat-related mortality in New York City, 1997–2006. Health & Place, 30, 45-60.

Kong, J., Zhao, Y., Strebel, D., Gao, K., Carmeliet, J., & Lei, C. (2023). Understanding the impact of heatwave on urban heat island in Greater Sydney: Temporal surface energy budget change with land types. *Journal of Urban Climate*, *44*, 101234. https://doi.org/10.1016/j.uclim.2023.101234

Oke, T. R. (1982). The energetic basis of the urban heat island. Quarterly Journal of the Royal Meteorological Society, 108(455), 1-24.

Oke, T. R. (1987). Boundary layer climates. Routledge.

Ramamurthy, P., & Bou-Zeid, E. (2016). Heatwaves and urban heat islands: A comparative analysis of multiple cities. *Journal of Climate*, *29*(24), 8629-8646. https://doi.org/10.1175/JCLI-D-16-0150.1

Rajeswari, R., Devara, P. C. S., Kishore Kumar, K., & Bhaskaran, B. (2021). Impact of urbanization on boundary layer characteristics over a coastal city in the tropical region. Meteorology and Atmospheric Physics, 133(3), 393-408.

Roth, M. (2000). Review of atmospheric turbulence over cities. Quarterly Journal of the Royal Meteorological Society, 126(564), 941-990.

Roukounakis, N.; Varotsos, K.V.; Katsanos, D.; Lemesios, I.; Giannakopoulos, C.; Retalis, A. (2023) High Resolution WRF Modelling of Extreme Heat Events and Mapping of the Urban Heat Island Characteristics in Athens, Greece. *Sustainability* 2023, *15*, 16509. https://doi.org/10.3390/su152316509

Rui Silva, Ana Cristina Carvalho, Susana Cardoso Pereira, David Carvalho, Alfredo Rocha, (2022) Lisbon urban heat island in future urban and climate scenarios,Urban Climate,Volume 44,2022,101218,ISSN 2212-0955,

Url-1 < https://data.worldbank.org/country/Türkiye

Url-2 <https://doi.org/10.1016/j.uclim.2022.101218

World Meteorological Organization. (2023). https://public.wmo.int/en/our-mandate/focus-areas/weather/heatwaves

Saka, F. B. and Unal, Y. (2024) How does urbanization shape the record-breaking temperatures in Izmir, Turkey ?, EGU General Assembly 2024, Vienna, Austria, 14–19 Apr 2024, EGU24-15662, https://doi.org/10.5194/egusphere-egu24-15662, 2024.

Salamanca, F., Krpo, A., Martilli, A., Clappier, A., & Erell, E. (2014). A methodology for the retrieval of the urban heat island signature from earth observation data. Remote Sensing of Environment, 142, 10-20.

Smith, A. B., Bornstein, R. D., & Westerling, A. L. (2015). Use of the Weather Research and Forecasting model for predicting urban heat: A sensitivity study. Journal of Applied Meteorology and Climatology, 54(1), 180-194.

Stefanon, M., D'Andrea, F., & Drobinski, P. (2012). Heatwave classification over Europe and the Mediterranean region. *Environmental Research Letters*, 7(1), 014023. https://doi.org/10.1088/1748-9326/7/1/014023

Stull, R. B. (1988). An Introduction to Boundary Layer Meteorology. Springer.

Taylor, K. E. (2001). Summarizing multiple aspects of model performance in a single diagram. Journal of Geophysical Research: Atmospheres, 106(D7), 7183-7192. https://doi.org/10.1029/2000JD900719

Ünal, Y. S., Tan, E., & Mentes, S. S. (2013). Summer heat waves over western Turkey between 1965 and 2006. Theoretical and Applied Climatology, 112(1–2), 339–350. https://doi.org/10.1007/s00704-012-0704-0

Ünal, Y. S., Sonuç, C. Y., Incecik, S., Topcu, H. S., Diren-Üstün, D. H., & Temizöz, H. P. (2020). Investigating urban heat island intensity in Istanbul. *Theoretical and Applied Climatology*, *139*(1–2), 175–190. https://doi.org/10.1007/s00704-019-02953-2

Zhang, R., Lei, Y., Qiu, L., Lei, T., Li, C., & Li, X. (2019). Urban air pollution in China: Current status, characteristics, and progress. Annual Review of Energy and the Environment, 44(1), 309-339.

Özdemir, H., Togan, V., Yılmaz, H., & Çelik, A. (2020). Urban heat islands and heatwaves in Istanbul. Hittite Journal of Science and Engineering, 7(1), 61-68.

Ventura, S., Miró, J.R., Peña, J.C. et al. (2023) Analysis of synoptic weather patterns of heatwave events. Clim Dyn 61, 4679–4702 (2023). https://doi.org/10.1007/s00382-023-06828-1

Yücel, İ., Ünal, Y. Y., & Türkeş, M. (2017). Observed trends and variability of extreme climate events in Türkiye. International Journal of Climatology, 37(3), 1384-1397.

APPENDIX

APPENDIX A : WRF Model namelist input setup

APPENDIX B : CORINE Landuse data categories

APPENDIX A

```
&time_control
 run_days                  = 30,
 run_hours                 = 23,
 run_minutes               = 0,
 run_seconds               = 0,
 start_year                = 2023, 2023,
2023,
 start_month               = 07,   07,
07,
 start_day                 = 01,   01,
01,
 start_hour                = 00,   00,
00,
 start_minute              = 00,   00,
00,
 start_second              = 00,   00,
00,
 end_year                  = 2023, 2023,
2023,
 end_month                 = 07,   07,
07,
 end_day                   = 30,   30,
30,
 end_hour                  = 23,   23,
23,
 end_minute                = 00,   00,
00,
 end_second                = 00,   00,
00,
 interval_seconds          = 3600
 input_from_file           =
.true.,.true.,.true.,
 history_interval          = 180,  60,
60,
 frames_per_outfile        = 170,
170, 170,
 restart                   = .false.,
 restart_interval          = 5000,
 io_form_history           = 2
 io_form_restart           = 2
 io_form_input             = 2
 io_form_boundary          = 2
 debug_level               = 100
 /

 &domains
 time_step                 = 54
 time_step_fract_num       = 0,
 time_step_fract_den       = 1,
 max_dom                   = 3,
 e_we                      = 76,    109,
202,
 e_sn                      = 76,    109,
202,
 e_vert                    = 61,    61,
61,
 p_top_requested           = 5000,
 num_metgrid_levels        = 38,
 num_metgrid_soil_levels   = 4,
 dx                        = 9000, 3000,
1000,
```

dy = 9000, 3000, 1000,
grid_id = 1, 2, 3,
parent_id = 1, 1, 2,
i_parent_start = 1, 20, 20,
j_parent_start = 1, 20, 20,
parent_grid_ratio = 1, 3, 3,
parent_time_step_ratio = 1, 3, 3,
feedback = 1,
smooth_option = 0
eta_levels = 1.000000, 0.998600, 0.996000, 0.994000, 0.992000,
0.990000, 0.987592, 0.984486, 0.980977, 0.977016,
0.972544, 0.967500, 0.961813, 0.955403, 0.948185,
0.940062, 0.930929, 0.920670, 0.909158, 0.896257,
0.881820, 0.859633, 0.830162, 0.794019, 0.751945,
0.704330, 0.659043, 0.615990, 0.575078, 0.536219,
0.499329, 0.464324, 0.431126, 0.399657, 0.369845,
0.341616, 0.314904, 0.289641, 0.265763, 0.243210,
0.221922, 0.201841, 0.182641, 0.164410, 0.148206,
0.132526, 0.117709, 0.104002, 0.091398, 0.079808,
0.069150, 0.059351, 0.050340, 0.042054, 0.034434,
0.027428, 0.020986, 0.015062, 0.009615, 0.004606,
0.000000
/

&physics
mp_physics = 2, 2, 2,
ra_lw_physics = 1, 1, 1,
ra_sw_physics = 1, 1, 1,
radt = 30, 30, 30,
sf_sfclay_physics = 5, 5, 5,
sf_surface_physics = 2, 2, 2,
bl_pbl_physics = 5, 5, 5,
bldt = 0, 0, 0,
cu_physics = 1, 0, 0,
cudt = 5, 5, 5,
isfflx = 1,
ifsnow = 1,
icloud = 1,
surface_input_source = 1,
num_soil_layers = 4,
num_land_cat = 28,
sf_urban_physics = 1, 1, 1,
sf_surface_mosaic = 0,
mosaic_cat = 3,

APPENDIX B

Figure B.1 : CORINE Landuse data categories.

CURRICULUM VITAE

Name Surname **:** Fatma Başak SAKA

EDUCATION:

- **B.Sc.** **:** 2016, Istanbul Technical University, Meteorological Engineering Department
- **M.Sc.** **:** 2024, Istanbul Technical University, Meteorological Engineering Department

PROFESSIONAL EXPERIENCE AND REWARDS:

- 2022- … Jr. Energy Meteorologist, EDF Trading
- 2021-2022 Meteorological Engineer, Aigoritma
- 2020-2021 Part Time Operational Meteorologist, Borusan ENBW Energy

PUBLICATIONS, PRESENTATIONS AND PATENTS ON THE THESIS:

- **Saka, F. B**. and Unal, Y.: How does urbanization shape the record-breaking temperatures in Izmir, Turkey ?, EGU General Assembly 2024, Vienna, Austria, 14–19 Apr 2024, EGU24-15662, https://doi.org/10.5194/egusphere-egu24-15662, 2024. (Poster Presentation)

OTHER PUBLICATIONS, PRESENTATIONS AND PATENTS:

- **Saka, F. B.**, Ustun, H.D Unal, Y, 2021, Urban Heat Island Effect on Convective Precipitation Event in Izmir, Turkey, 8th International Conference on Meteorology and Climatology of the Mediterranean (MetMed) (Oral Presentation)
- **Saka, F. B.**, Dinç, U., Kara, Y., Ünal, Z. F., Akalın, I. A., Öztürk, B., & Toros, H. (2019). Thunderstorm modeling with WRF: Parameterization study for Istanbul. Poster presented at The Royal Meteorological Society (RMetS) Virtual Student & Early Career Scientists Conference.